Zhang et al. *Zool. Res.* 2025, 46(6): 1531−1548
https://doi.org/10.24272/j.issn.2095-8137.2025.032
https://cstr.cn/32248.14.zr.2025.032

ZR | Zoological Research

Article Open Access

Rescuing fertility: C-Phycocyanin prevents ovarian damage through NRF2-mediated ferroptosis pathways in polycystic ovary syndrome models

Jing Zhang[1,2,#], Qun-Shan Shen[1,3,#], Ya-Xin Chen[1,3,#], Hui-Ru Cheng[1,3], Wei Zhang[1,3], Ting Xing[1,3], Ya-Jing Liu[1,3], Yun-Xia Cao[1,3], Dan Liang[1,3], Man Luo[4,5,*], Biao Yu[1,3,*]

[1] *Department of Obstetrics and Gynecology*, *NHC Key Laboratory of Study on Abnormal Gametes and Reproductive Tract*, *First Affiliated Hospital of Anhui Medical University*, *Hefei*, *Anhui* 230022, *China*

[2] *College of Grain Engineering*, *Anhui Vocational College of Grain Engineering*, *Hefei*, *Anhui* 230011, *China*

[3] *Engineering Research Center of Biopreservation and Artificial Organs*, *Ministry of Education*, *Hefei*, *Anhui* 230032, *China*

[4] *Department of Obstetrics and Gynecology*, *Zhengzhou Central Hospital Affiliated to Zhengzhou University*, *Zhengzhou*, *Henan* 450007, *China*

[5] *Zhengzhou City Key Laboratory of Endocrine Metabolism and Immunity in Polycystic Ovary Syndrome*, *Zhengzhou*, *Henan* 450007, *China*

ABSTRACT

Polycystic ovary syndrome (PCOS), a common female endocrine disorder marked by disrupted folliculogenesis and hyperandrogenism, is increasingly linked to oxidative stress. Despite this association, the mechanistic basis remains poorly characterized. C-Phycocyanin (C-PC), a cyanobacteria-derived protein with potent antioxidant properties, has demonstrated therapeutic potential for treating PCOS, though the molecular pathways mediating its effects have yet to be delineated. This study employed both a dehydroepiandrosterone (DHEA)-induced murine model and DHEA-challenged human granulosa cells (KGN) to elucidate the regulatory role of C-PC. *In vivo*, oral administration of C-PC restored estrous cyclicity, reduced the prevalence of cystic follicles, and normalized circulating levels of testosterone, estradiol, progesterone, and luteinizing hormone (LH). *In vitro*, C-PC treatment activated the NRF2/xCT/GPX4 pathway, enhanced antioxidant activity, improved mitochondrial function, and suppressed ferroptotic death. Direct molecular interaction between C-PC and NRF2 was validated through molecular docking and cellular thermal shift assays (CETSA). Correspondingly, *in vivo* administration alleviated oxidative stress, inhibited ferroptosis, and increased GPX4 and xCT expression, effects reversed by pharmacological inhibition (ML385) and genetic silencing (AAV-sh-NRF2) of NRF2. C-PC also reduced DHEA-induced phosphorylation of AMPK, while co-treatment with an AMPK activator attenuated its effects on GPX4 and xCT, abolishing its anti-ferroptotic protection against granulosa cells. These findings suggest that C-PC mitigates PCOS pathology by repressing granulosa cell ferroptosis through coordinated activation of NRF2 and modulation of redox-sensitive AMPK signaling, highlighting its potential as a redox-targeted therapeutic strategy for PCOS.

Keywords: Polycystic ovary syndrome (PCOS); C-Phycocyanin (C-PC); Nuclear factor erythroid 2-related factor 2 (NRF2); Antioxidant; Ferroptosis

INTRODUCTION

Polycystic ovary syndrome (PCOS) represents the most prevalent endocrine disorder among reproductive-age females, affecting over 5% of this population globally (Azziz et al., 2004). Clinically, PCOS is defined by chronic anovulation, menstrual irregularities such as oligomenorrhea or amenorrhea, and androgen excess, frequently accompanied by metabolic dysfunctions including obesity, insulin resistance, increased cardiovascular risk, and subfertility (Goodarzi et al., 2011; Sadeghi et al., 2022). Histologically, it is characterized by stromal hyperplasia and thecal cell expansion within the ovaries, leading to excessive

This is an open-access article distributed under the terms of the Creative Commons Attribution Non-Commercial License (http://creativecommons.org/licenses/by-nc/4.0/), which permits unrestricted non-commercial use, distribution, and reproduction in any medium, provided the original work is properly cited.

Copyright ©2025 Editorial Office of Zoological Research, Kunming Institute of Zoology, Chinese Academy of Sciences

Received: 02 August 2025; Accepted: 15 September 2025; Online: 16 September 2025

Foundation items: This work was supported by the National Natural Science Foundation of China (82501986), Anhui Provincial Natural Science Foundation Youth Project (2508085QE176), Anhui Key Project Fund for College and University (2024AH050713), and Henan Provincial Department of Science and Technology (252300421643)

[#]Authors contributed equally to this work

*Corresponding authors, E-mail: biaoyu@ahmu.edu.cn; luomanzz@zzu.edu.cn

androgen biosynthesis and follicular arrest with cyst formation (Amin et al., 2003). Beyond reproductive and metabolic manifestations, PCOS imposes substantial psychological burdens, including anxiety and depression, which further impair patient quality of life (Rzońca et al., 2018). Despite extensive investigation, the etiology of PCOS remains unclear, underscoring its multifactorial and heterogeneous nature. However, increasing evidence suggests that chronic, low-grade systemic and ovarian inflammation and oxidative stress are associated with PCOS and its related endocrinological dysfunction (Huang et al., 2022; Luo et al., 2020b, 2021; Wang et al., 2024b). Contributing factors include hyperglycemia, hyperlipemia, hyperinsulinemia, hyperandrogenemia, abdominal adiposity, and obesity, all of which exacerbate redox imbalance (Liu et al., 2010). This persistent oxidative burden has been identified as a critical mediator of follicular dysfunction and anovulation in PCOS.

Elevated reactive oxygen species (ROS) levels directly impair oocyte maturation, meiotic integrity, and developmental competence (Goud et al., 2008). Both clinical and experimental studies suggest that oxidative stress induced by ROS plays a critical role in the pathophysiology of fertility-related diseases, including PCOS, infertility, and endometriosis (Agarwal et al., 2012). Pharmacological agents with antioxidant properties, such as rosiglitazone, metformin, and melatonin, have demonstrated beneficial effects on fertility- related disorders through reductions in ROS levels (Yilmaz et al., 2005). These observations highlight the need for detailed characterization of ROS generation and regulatory pathways in PCOS to guide the development of effective preventive and therapeutic strategies.

Ferroptosis is a regulated form of cell death driven by iron-dependent lipid peroxidation and the uncontrolled accumulation of ROS and lipid peroxides (Bersuker et al., 2019; Stockwell et al., 2017). Key regulators of this process include glutathione peroxidase 4 (GPX4) and the cystine/glutamate transporter xCT (encoded by SLC7A11), which together maintain redox homeostasis by reducing lipid hydroperoxides to nontoxic lipids (Yang et al., 2014; Zhang et al., 2021). Disruptions in glutathione (GSH) synthesis or inhibition of xCT or GPX4 can compromise this defense system, triggering ferroptotic death, particularly under conditions of intracellular iron overload (Abdalkader et al., 2018). Nuclear factor erythroid 2-related factor 2 (NRF2) has emerged as a key regulator of cellular antioxidant responses, redox homeostasis, and inflammation (Dodson et al., 2019; Ma et al., 2020). By transcriptionally activating a suite of cytoprotective genes, including xCT and GPX4, NRF2 plays a protective role against ferroptosis, oxidative damage, and inflammatory stress (Ananth et al., 2021). Accumulating evidence suggests that ferroptosis is involved in the pathophysiology of various chronic diseases, underscoring the broad relevance of NRF2-driven redox regulation as a conserved mechanism of cellular defense against ferroptotic injury.

Recent evidence has increasingly implicated granulosa cell (GC) ferroptosis, driven by excessive ROS, as a key pathological mechanism underlying impaired follicular development and reduced fertility in PCOS (Li et al., 2024a; Merhi et al., 2019; Yan et al., 2024). Ferroptosis, an iron-catalyzed, lipid peroxidation-dependent mode of cell death, is closely linked to redox imbalance and is particularly pronounced in PCOS ovaries (Li et al., 2020). Aberrant ROS accumulation in experimental PCOS models has been shown to damage cellular structures and drive lipid peroxidation, thereby promoting ferroptotic degeneration of GCs (Zhang et al., 2023). Conversely, pharmacological inhibition of ferroptosis using agents such as ferrostatin-1 has been demonstrated to attenuate ROS accumulation, reduce lipid peroxidation, and improve ovarian morphology and function (Li et al., 2024b). Under physiological conditions, ROS levels are tightly regulated by both enzymatic and nonenzymatic antioxidant defense systems, including superoxide dismutase (SOD), catalase (CAT), and glutathione peroxidase (GPx) (Irato & Santovito, 2021). In PCOS, however, this redox defense network is frequently compromised. Clinical and preclinical studies of PCOS have consistently reported reduced expression and enzymatic activity of SOD, CAT, and GPx in both serum and ovarian tissue, resulting in an oxidant-rich microenvironment conducive to ferroptotic activation (Chen et al., 2025; Khadrawy et al., 2019). Furthermore, recent research has suggested the existence of a self-reinforcing feedback loop wherein ROS accelerates ferroptosis via lipid peroxidation, and ferroptosis amplifies ROS generation through the degradation of mitochondrial and membrane lipids (Su et al., 2019; Wang et al., 2023). This feed-forward circuit intensifies cellular damage and follicular dysfunction. As such, therapeutic strategies targeting ROS-mediated ferroptosis, such as antioxidant supplementation or ferroptosis blockade, are being explored as promising avenues for improving ovarian function in PCOS.

C-Phycocyanin (C-PC), a biliprotein derived from cyanobacteria, is widely used as a nutritional supplement and exhibits a broad spectrum of pharmacological activities (Kuddus et al., 2013; Patil et al., 2006; Yoshida et al., 1996), including antioxidant, anti-inflammatory, antitumor, and antiallergic effects (Li et al., 2013; Piovan et al., 2022; Romay et al., 2003; Roy et al., 2007; Wu et al., 2016). Its intense blue pigmentation arises from the phycocyanobilin chromophore, a linear tetrapyrrole covalently bound to alpha (α) and beta (β) protein subunits. C-PC has been shown to exert anti-inflammatory effects by selectively inhibiting COX-2 (Reddy et al., 2000), inhibiting NF-κB signaling and consequent inflammatory mediator release (Sun et al., 2011), and scavenging ROS to attenuate oxidative injury (Bhat & Madyastha, 2000).

This study investigated the role of C-PC in regulating oxidative stress and endocrine dysfunction in a dehydroepiandrosterone (DHEA)-induced PCOS mouse model, evaluated whether C-PC supplementation attenuated oxidative injury and improved PCOS-related hormonal abnormalities, and determined whether these actions were mediated through the NRF2 signaling pathway. These investigations revealed that C-PC confers protective effects against PCOS-related oxidative and endocrine disruptions by engaging NRF2-driven ferroptosis resistance, establishing a mechanistic framework for its therapeutic potential in redox-impaired ovarian pathologies.

MATERIALS AND METHODS

Chemicals and reagents

C-PC (P2172), ferroptosis inhibitor ferrostatin-1 (Fer-1; SML0583, Sigma, US), antioxidant N-acetyl-L-cysteine (NAC; A7250; Sigma, US), and specific NRF2 inhibitor ML385 were obtained from KKL Med (KM3775; China). Cell Counting Kit-8

(CCK-8) (HY-K0301) was obtained from MedChemExpress (USA). Various antibodies were purchased, including antibodies against 4-HNE (bs-6313R; Bioss, China), histone H3 (4499; Cell Signaling Technology, USA), β-actin (66009-1; Proteintech, China), xCT/SLC7A11 (26864-1; Proteintech, China), HO-1 (10701-1; Proteintech, China), GPX4 (YM8430; Immunoway, USA), and NRF2 (GTX103322; GeneTex, USA). All chemical reagents used were of analytical grade.

Mice and animal procedures

All protocols involving animals were approved by the Association of Laboratory Animal Sciences at Anhui Medical University (Approval No. LLSC20241895) and were carried out in strict accordance with the National Institutes of Health Guide for the Care and Use of Laboratory Animals (NIH Publication, 8th Edition, 2011). Twenty-five-day-old female ICR mice were obtained from GemPharmatech (China). Upon arrival, the mice were provided *ad libitum* access to food and water under controlled conditions (20–22°C, 50%–60% relative humidity, 12 h light/dark cycle).

To induce a PCOS phenotype, mice were subcutaneously injected with dehydroepiandrosterone (DHEA, 6 mg/100 g body weight, 0.1 mL/mouse in sesame oil with 10% of 95% ethanol, LKT Laboratories, USA) for 3 consecutive weeks, as described previously (Luo et al., 2020a). C-PC (500 mg/kg in sterile double-distilled water, 0.1 mL/mouse) was intragastrically administered for 4 consecutive weeks, with daily inspection of the estrous cycle (Ou et al., 2012; Yang et al., 2022) . Control mice received equivalent volumes of vehicle for an equivalent length of time. After treatment, ovaries and orbital blood were collected.

To investigate the involvement of NRF2, PCOS model mice were randomly assigned to two groups. As described previously (Luo et al., 2024), the AAV-sh-NC group received an intravenous injection of adeno-associated virus (AAV, IDMO, China) carrying a negative control (NC) plasmid with the sequence TTCTCCGAACGTGTCACGTAA. The AAV-sh-NRF2 group received an intravenous injection of AAV vector carrying the sh-NRF2 plasmid with the sequence CTTGAAGTCTTCAGCATGTTA. Vectors were administered via tail vein injection at a concentration of 1×10^{12} AAV (v.g./mL/mouse). Two weeks post-injection, mice received dietary supplementation with C-PC (500 mg/kg/day) for 4 consecutive weeks. Ovarian tissues were collected for histological evaluation and molecular analysis following treatment.

Open field test (OFT)

To assess anxiety-like behavior in the mice, the mice were placed on the center area of an open field device under dim light consisted of an open box 50 cm long × 50 cm wide × 25 cm high, and then the mice were allowed to explore freely for 5 min. The total traveled distance, the distance traveled in the center zone, the velocity, the time spent in the center zone, the time spent in surrounding zone, and the distance traveled in surrounding zone were recorded to assess anxiety-like behavior in mice using ANY-Maze software (Stoeling, USA). After each mouse, the box was washed with 75% alcohol to eliminate the odor of the last mouse.

Vaginal smear analysis

Vaginal smears were collected daily to monitor estrous cyclicity. A moistened cotton swab was gently inserted into the vaginal opening to obtain epithelial cells, which were transferred to glass slides, air-dried, and stained using Giemsa solution (Baso Biotechnology, China) according to the manufacturer's instructions. Estrous stages were determined by microscopy based on the dominant cell population. The four phases of the mouse estrous cycle were classified as follows: (a) Proestrus (P): Predominance of nucleated epithelial cells; (b) Estrus (E): Predominance of cornified keratinocytes; (c) Metestrus (M): Mixed population of epithelial cells, keratinocytes, and leukocytes; and (d) Diestrus (D): Predominance of leukocytes.

Fertility assessment

To assess reproductive capacity, DHEA-induced PCOS females were co-housed with proven fertile ICR males (1:1 ratio) overnight. Successful mating was confirmed by the presence of a vaginal plug the following morning. Plug-positive females were then housed individually, and reproductive parameters including mating rate, pregnancy rate, litter size, and time to first litter were recorded.

Hematoxylin and eosin (H&E) staining and follicle quantification

Ovarian tissues were processed for paraffin embedding, serially sectioned, and stained with H&E (G1126; Solarbio, China) following standard protocols (Yu et al., 2023). Histological evaluation was performed by independent researchers in a blinded manner. To avoid double counting, only follicles containing a visible oocyte nucleus were included. Follicles were classified based on Pederson's criteria: primordial follicles contained a single layer of flattened GCs; primary follicles contained a single layer of cuboidal GCs; secondary follicles had two or more layers of cuboidal GCs without a visible antrum; and antral follicles exhibited a well-defined fluid-filled cavity. Every fifth section was analyzed (as the same follicle will appear on neighboring slices), and total follicle counts were calculated as the sum across all identified stages per ovary.

Enzyme-linked immunosorbent assay (ELISA)

Orbital blood was collected during the diestrus phase to minimize hormonal variability and improve the accuracy of hormonal analysis. Serum levels of testosterone (T, CSB-E05101m), estradiol (E2, CSB-E05109m), progesterone (P4, CSB-E05104m), follicle-stimulating hormone (FSH, CSB-E06871m), and luteinizing hormone (LH, CSB-E12770m) were quantified using the corresponding ELISA kits (Cusabio, China) according to the manufacturer's instructions.

Quantification of malondialdehyde (MDA), superoxide dismutase (SOD), and catalase (CAT)

Ovarian MDA levels were assessed using an MDA (LV30953) assay kit (Aimeng Youning, China). SOD (A001) and CAT (A007) levels were measured using commercial kits from Jiancheng Biology Engineering Institute (China). Optical density (OD) was determined using a microplate reader at 450 nm. Protein concentrations were assayed using a BCA protein quantification kit (P0010; Beyotime, China).

Cell culture

The human ovarian GC line (KGN, ATCC, RRID: CVCL_0603) was obtained from the Cell Bank of the Chinese Academy of Sciences (China) and cultured in Dulbecco's Modified Eagle Medium (DMEM; HyClone, USA) supplemented with 10% fetal bovine serum (FBS; Gibco, USA), penicillin (100 IU/mL), and streptomycin sulfate (100 μg/mL) at 37°C in a 5% CO_2

incubator. Cells were pretreated with 5 μmol/L C-PC for 2 h, followed by treatment with 10 μmol/L DHEA for 48 h.

Measurement of reduced glutathione (GSH) and oxidized glutathione (GSSG) levels

Intracellular GSH and GSSG levels were quantified in GCs following protein extraction and normalization, using a commercial GSH/GSSG Assay Kit (S0053; Beyotime, China) in accordance with the manufacturer's instructions.

CCK8 and lactate dehydrogenase (LDH) assays

Cell viability was assessed using the CCK-8 assay. Briefly, KGN cells (1×10^4 cells/well) were seeded in 96-well plates and treated with C-PC for 24 h. Subsequently, 10 μL of CCK-8 reagent was added to each well and incubated for 1.5 h at 37°C. Absorbance was measured at 450 nm using a microplate reader (Bio-Rad, USA). LDH release was assessed as a marker of cytotoxicity using supernatants collected from each group. LDH levels were measured using a commercial kit (Jiancheng Bioengineering Institute, China) according to the manufacturer's instructions.

Caspase 3 activity assay

Caspase-3 enzymatic activity was assessed using a colorimetric detection kit (Beyotime, China). Following cell lysis, samples were incubated with Ac-DEVD-pNA substrate at 37°C for 2 h. Absorbance was recorded at 405 nm, and caspase-3 activity was normalized to untreated controls.

Flow cytometric detection of ROS

Intracellular ROS levels were determined using a fluorescent probe (D6883; 2',7'-dichlorofluorescein diacetate; DCFH-DA; Sigma, China). KGN cells cultured in a 6-well plate were exposed to DHEA for 48 h, followed by incubation with 2 μmol/L DCFH-DA at 37°C for 20 min. Fluorescence intensity was quantified by flow cytometry (Beckman Coulter, USA), and data were analyzed using FlowJo v.7.6 software.

Fluorescence imaging of ROS and lipid ROS

ROS levels were determined using the fluorescent probe dihydroethidium (DHE; S0063; 5 μmol/L; Beyotime, China) for 20 min at 37°C. Increased red fluorescence intensity indicated higher ROS levels. Lipid peroxidation was assessed by determining lipid ROS levels with the BODIPY™ 493/503 probe (5 μmol/L; CM02294; Proteintech, China). After 30 min incubation in the dark at 37°C, cells were imaged with a confocal microscope (Olympus, Japan). ImageJ v.1.45s was used to quantify fluorescence intensity for both ROS and lipid ROS.

Western blotting

Proteins were extracted from mouse ovaries and cultured cells using M-PER™ Mammalian Protein Extraction Reagent (78501; Thermo, USA). Protein concentrations were determined using a BCA Protein Assay Kit (Beyotime, China). Equal amounts of protein were separated by sodium dodecyl sulfate-polyacrylamide gel electrophoresis (SDS-PAGE) and transferred to polyvinylidene fluoride (PVDF) membranes (Millipore, USA). Membranes were blocked with 5% non-fat milk in Tris-Buffered Saline with Tween 20 (TBST) for 1 h at room temperature, followed by overnight incubation at 4°C with primary antibodies. After washing, membranes were incubated with horseradish peroxidase (HRP)-conjugated secondary antibodies and visualized using enhanced chemiluminescence (ECL) reagents (1512402; Millipore, USA). Band intensities were quantified using ImageJ v.1.45s (NIH, USA).

Immunofluorescence staining

GCs and ovaries were fixed in 4% paraformaldehyde (PFA; G1101; Servicebio, China) for 15 min and treated with blocking buffer (0.2% sodium azide, 2% bovine serum albumin (BSA), and 0.1% Triton X-100 in TBST) for 1 h. Samples were incubated with rabbit anti-NRF2, anti-GPX4, and anti-xCT (1:200 dilution) antibodies at 4°C overnight. Slides were mounted with DAPI mounting solution (1:500 dilution; D9542; Sigma Aldrich, USA) for 5 min and photographed using an Olympus microscope. Fluorescence intensity was calculated using ImageJ v.1.45s.

Chromatin immunoprecipitation-quantitative real-time polymerase chain reaction (ChIP-qPCR)

The interaction between NRF2 and *GPX4* and *xCT* promoters was analyzed using a Pierce™ Agarose ChIP Kit (26156; Thermo Fisher, USA). Protein-DNA crosslinking was achieved using 4% PFA. After ultrasonic fragmentation, the complexes were immunoprecipitated with primary antibodies against rabbit NRF2 or rabbit IgG. The cross-linked complexes were extracted, solubilized, and subjected to qPCR to quantify the enrichment of *GPX4* and *xCT* promoter regions.

Oxygen consumption rate (OCR) and extracellular acidification rate (ECAR)

Mitochondrial OCR and ECAR were measured using a Seahorse XF24 Extracellular Flux Analyzer (Seahorse Bioscience, USA) following the manufacturer's instructions. Cells were seeded into XF24 cell culture microplates at a density of 2×10^4 cells/well and continuously incubated for 24 h. Cells were sequentially treated with ATP synthase inhibitor oligomycin A (2 μmol/L), ATP synthesis uncoupler carbonyl cyanide-4-trifluoromethoxyphenylhydrazone FCCP (1.5 μmol/L), complex I inhibitor rotenone (2 μmol/L), and complex III inhibitor antimycin A (2 μmol/L). Basal OCR and ECAR were recorded in the absence of metabolic inhibitors.

Mitochondrial membrane potential (MMP) analysis

Following treatment, GCs were incubated with JC-1 staining solution (C2003S; Beyotime, China) to assess MMP. Fluorescence was measured using flow cytometry (Beckman Coulter, USA), and red-to-green fluorescence ratios were used to quantify changes in MMP.

Molecular dynamics simulations and molecular docking

The NRF2 protein model was generated using AlphaFold2 (Zweckstetter, 2021), and simulations were performed in Desmond v.6.6 using the OPLS4 force field. A cubic simulation box (1 nm^3) was solvated with TIP3P water and neutralized with Na^+/Cl^- at physiological (0.135 mol/L) and high (0.165 mol/L) salt concentrations. The pH level was set to 7.4. The system underwent 1 000 steps of energy minimization using the conjugate gradient method, followed by heating to 303.15 K under canonical ensemble (NVT) conditions, with an integration time step of 1 fs and a total heating duration of 100 ps. The system was equilibrated for 50 ps, followed by a 50 ns protein simulation. Structural analysis was performed with Desmond and PyMOL v.2.4 (Schiffrin et al., 2020). Protein-ligand interactions were analyzed using Ligplot (Narayanan & Dias, 2013), and distance-related plots were generated using Desmond. Protein binding energy and virtual screening were conducted using Rosetta Flex ddG (Barlow et al., 2018).

Molecular docking analysis was employed to investigate the binding affinity of C-PC to NRF2. The crystal structure of NRF2 (PDB ID: 2OBI) was obtained from the Protein Data Bank (https://www.rcsb.org/) and the structure of C-PC was obtained from the PubChem database (https://pubchem.ncbi.nlm.nih.gov/). Ligand and protein structures were prepared following standard procedures and subjected to molecular docking using AutoDock Vina (USA).

Cellular thermal shift assay (CETSA)

GCs were lysed in liquid nitrogen through three cycles of freezing and thawing. Lysates were centrifuged at 12 000 ×*g* for 15 min at 4°C to collect supernatants, which were divided into two groups and incubated with or without C-PC at 25°C for 30 min. Samples were then divided into five equal groups and heated at 45°C, 50°C, 55°C, 60°C, or 65°C for 3 min. After cooling to ambient temperature, the samples underwent an additional round of centrifugation at 12 000 ×*g* for 15 min at 4°C, with the resulting supernatants subjected to western blot analysis.

Iron quantification and ferrous ion staining

Total intracellular iron levels were measured using an Iron Assay Kit (Leagene, China) following the manufacturer's instructions. Absorbance values of the blank, iron standard solution, and test samples were determined, and the iron content in each group was quantified by colorimetric analysis.

Intracellular ferrous ion (Fe^{2+}) levels were assessed using the fluorescent probe FerroOrange (Dojindo Laboratories, Japan), according to the manufacturer's protocols. GCs were incubated with 2 μmol/L FerroOrange at 37°C for 30 min. Fluorescence images were captured using a confocal microscope (Carl Zeiss, Germany), and mean fluorescence intensity was quantified using ImageJ.

Quantitative real-time PCR (qPCR)

Total RNA (1 μg) was reverse transcribed using oligo(dT) primers and reverse transcriptase (R302-01, Vazyme, China). RT-qPCR was performed using a HiScript II One Step RT-qPCR SYBR Green Kit (Q221-01, Vazyme, China) on the Light-Cycler® 96 SW system (Roche, Switzerland). *GAPDH* was used as the internal reference. All reactions were run in triplicate and normalized to *GAPDH* using a threshold-based algorithm, providing arbitrary units representing relative levels. Primer sequences are listed in Supplementary Table S1.

Statistical analysis

Statistical analyses were conducted using GraphPad Prism v.8.0 (GraphPad Software, USA). Data are expressed as mean±standard deviation (SD). Statistical significance was determined using either two-tailed Student's *t*-tests (for two group comparisons) or one-way analysis of variance (ANOVA) followed by Tukey's *post hoc* test (for multiple group comparisons), with $P<0.05$ indicating statistical significance.

RESULTS

C-PC restores ovarian function in PCOS model mice

To evaluate the therapeutic efficacy of C-PC in a PCOS model, ICR mice were subcutaneously injected with DHEA dissolved in sesame oil containing 10% (v/v) 95% ethanol for 3 weeks, followed by intragastric administration of C-PC (500 mg/kg/day) for 4 continuous weeks (Figure 1A). Restoration of estrous cyclicity was confirmed by daily vaginal cytology, which showed normalized through all four phases of the cycle in C-PC-treated animals (Figure 1B). Histological analysis of ovarian sections stained with H&E showed marked improvement in ovarian morphology following C-PC treatment, characterized by reduced cystic follicles and the reappearance of corpora lutea, consistent with reestablished ovulatory and estrous cycling (Figure 1C, D; Supplementary Figure S1A). C-PC treatment also enhanced, indicating functional recovery of fertility. Concurrently, serum concentrations of LH/FSH, T, E2, and P4 were significantly reduced in the C-PC treatment group, reflecting normalization of the hormonal environment disrupted in PCOS (Figure 1E–I). Given that PCOS is frequently accompanied by neurobehavioral disturbances resembling anxiety and depression (Igbo et al., 2022; Pan et al., 2022; Yu et al., 2016), the OFT was employed to assess locomotor and anxiety-like behavior in mice. Compared to the DHEA group, C-PC-treated mice exhibited increased total distance traveled and locomotor velocity, indicative of reduced anxiety-like behavior and enhanced exploratory behavior (Figure 1J, K; Supplementary Figure S1B, C).

C-PC attenuates ovarian oxidative stress and ferroptosis in PCOS model mice

Oxidative stress, a consequence of disrupted redox homeostasis, plays an essential role in PCOS pathogenesis (Lu et al., 2018; Papalou et al., 2016). Given the emerging role of GC ferroptosis in driving ovarian dysfunction in PCOS (Tan et al., 2022; Zhang et al., 2023), we hypothesized that C-PC may ameliorate PCOS by inhibiting oxidative stress and ferroptosis in GCs. Western blot analysis revealed that treatment with C-PC in DHEA-induced PCOS mice markedly increased both total and nuclear NRF2 protein levels, with no significant change observed in cytoplasmic NRF2 levels. Concurrently, expression of GPX4 and xCT, key NRF2 target genes involved in ferroptosis defense, was also significantly up-regulated, further suggesting that C-PC alleviates oxidative stress and ferroptosis (Figure 2A, B; Supplementary Figure S2A, B). Immunofluorescence staining confirmed increased ovarian NRF2 and GPX4 expression following C-PC supplementation (Figure 2C; Supplementary Figure S2C). In addition, the expression of other ferroptosis-related marker genes, including *ACSL4* and *TFR1*, was assessed using RT-qPCR. Both genes were significantly down-regulated in the C-PC group, indicating suppression of ferroptosis (Supplementary Figure S2D). Additionally, levels of MDA, a byproduct of lipid oxidation and an established ferroptosis biomarker, were significantly reduced in ovarian lysates from C-PC-treated mice (Figure 2D). C-PC also enhanced antioxidant capacity, as evidenced by increased GSH, GSH/GSSG, CAT, and SOD levels in the ovaries of mice (Figure 2D; Supplementary Figure S2E). Collectively, these findings suggest that C-PC attenuates PCOS by suppressing oxidative stress and ferroptosis.

C-PC reduces oxidative stress and improves mitochondrial function *in vitro*

Progressive apoptosis of ovarian GCs has been implicated in anovulatory phenotypes characteristic of PCOS (Huang et al., 2021; Li et al., 2019). To determine the cytoprotective properties of C-PC on cell viability, GCs were exposed to various concentrations of C-PC (0, 2.5, 5, 10, 25, and 50 μmol/L) for 24 h. Cell viability, as assessed using the CCK-8 assay, was significantly reduced at higher concentrations in a dose-dependent manner (Figure 3A). However, pre-exposure to C-PC (0–10 μmol/L) for 2 h prior to DHEA (10 μmol/L, 48 h)

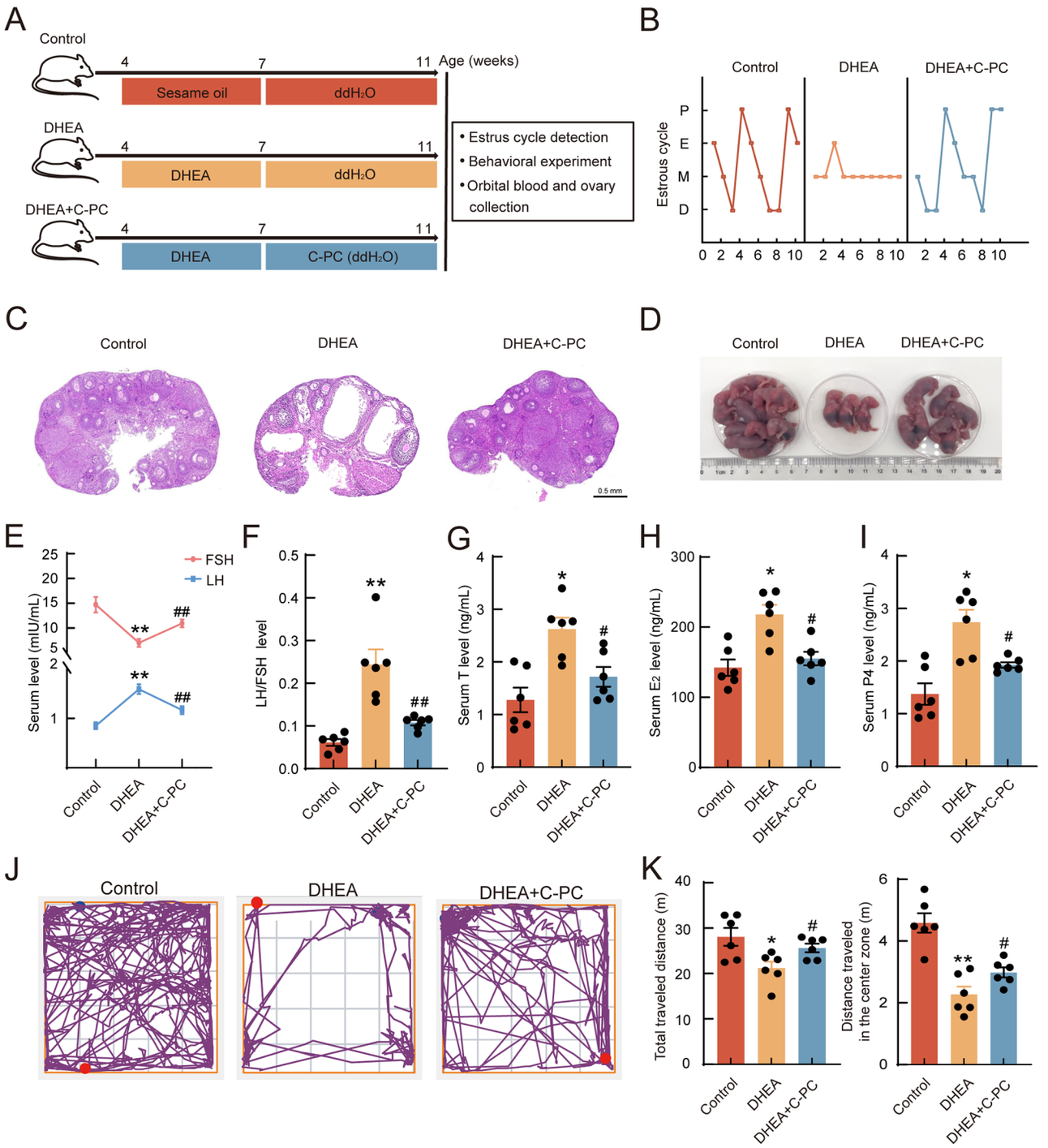


Figure 1 Oral administration of C-PC attenuates PCOS progression

A: Schematic of the experimental procedure. Mice received DHEA alone or DHEA in combination with C-PC and were assigned to Control, DHEA, and DHEA+C-PC groups. B: C-PC restored estrous cyclicity in PCOS mice. Ovaries were harvested for H&E staining and serum was collected for hormone analysis. Estrous cycle: proestrus (P), estrus (E), metestrus (M), and diestrus (D). C, D: Effects of C-PC on ovarian morphology and number of F1 in PCOS mice. Scale bar: 0.50 mm. E–I: Effects of C-PC on serum levels of T, P4, E2, LH, FSH, and LH/FSH ratio. J: Effect of C-PC treatment on exploratory activities and anxiety-like behaviors. K: Total distance traveled and distance traveled in center zone (n=6). Values are expressed as mean±SD. *: P<0.05, **: P<0.01; ***: P<0.001 vs. Control group; $^{\#}$: P<0.05; $^{\#\#}$: P<0.01 vs. DHEA group.

challenge resulted in increased protein expression of NRF2, HO-1, GPX4, and xCT (Figure 3B, C). Treatment with C-PC (5 μmol/L) significantly up-regulated the expression of NRF2 and GPX4 (Figure 3D–G). In parallel, transcriptional analysis by RT-qPCR revealed that C-PC treatment significantly down-regulated ferroptosis-related marker genes *ACSL4* and *TFR1*, indicating a potential inhibitory effect of C-PC on ferroptosis (Figure 3H). Consistent with this, C-PC markedly reduced oxidative stress-related proteins and lipid ROS accumulation, as demonstrated by immunofluorescence staining and flow cytometry analysis of DHEA-treated cells (Figure 3I–L).

Given the central role of mitochondria in regulating cellular energy metabolism and survival (Spinelli & Haigis, 2018), mitochondrial ultrastructure of GCs was examined by

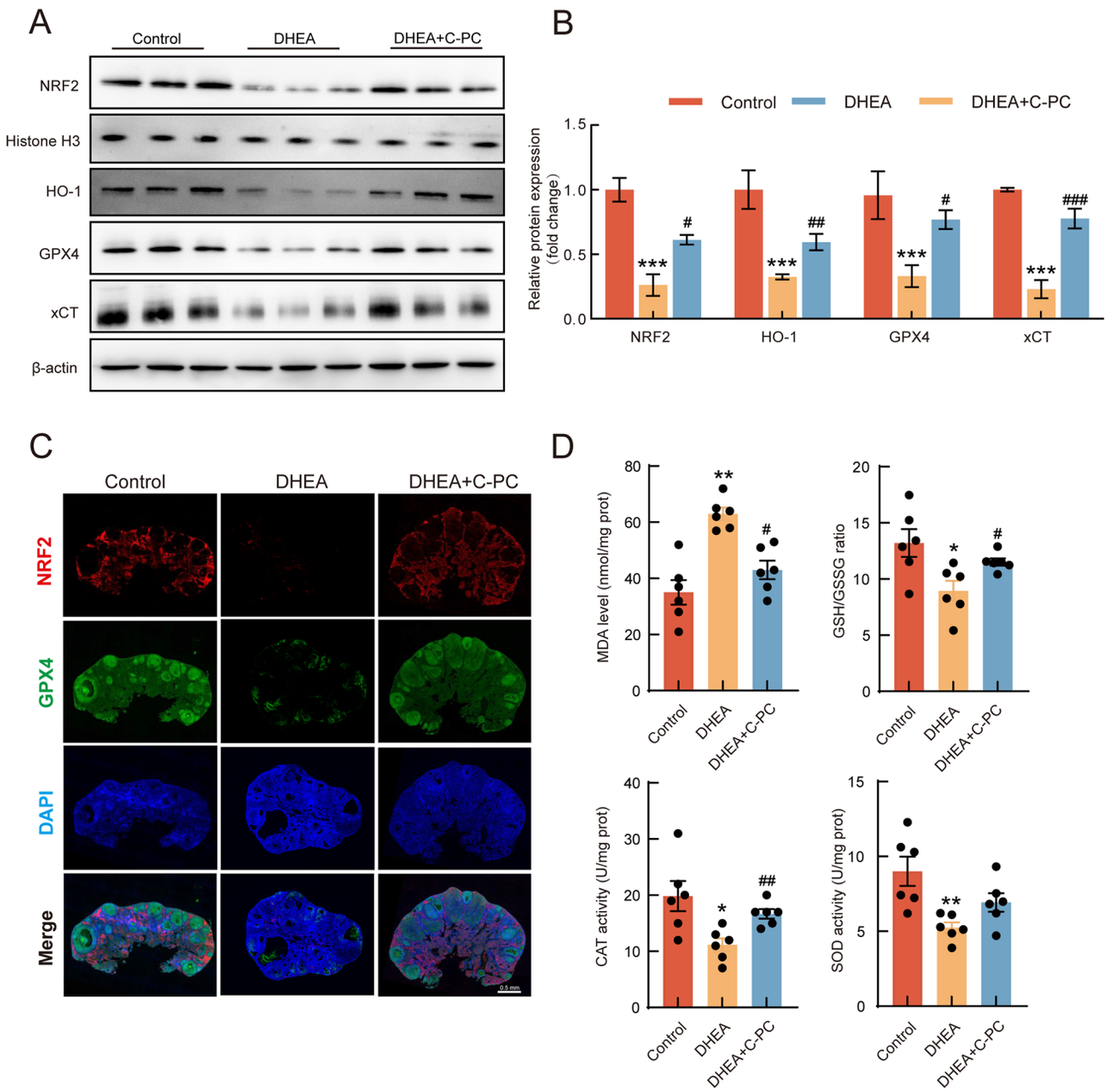


Figure 2 Oral administration of C-PC alleviates oxidative stress and ferroptosis in PCOS mice

A, B: Total and nuclear ovarian lysates were extracted from mice, and protein expression levels of GPX4, xCT, and NRF2 were detected (n=3). C: Confocal fluorescent staining was used to evaluate co-localization of GPX4 and NRF2 (n=3). D: MDA, GSH/GSSG ratio, CAT, and SOD levels in mouse ovarian lysates (n=6). Values are expressed as mean±SD. *: P<0.05; **: P<0.01; ***: P<0.001 vs. Control group; $^{\#}$: P<0.05; $^{\#\#}$: P<0.01; $^{\#\#\#}$: P<0.001 vs. DHEA group.

transmission electron microscopy (Figure 4A). Results demonstrated that DHEA exposure induced mitochondrial swelling, loss of cristae, and reduced organelle volume in GCs, whereas C-PC pretreatment preserved mitochondrial architecture and prevented structural deterioration (Figure 4B). Restoration of MMP was also observed in the C-PC-treated group, confirming functional rescue of mitochondrial activity (Figure 4C; Supplementary Figure S3A, B).

To further characterize iron homeostasis, intracellular total iron and ferrous ion (Fe^{2+}) levels were determined using a commercial assay and FerroOrange fluorescent probe, respectively. Both parameters were significantly elevated in the DHEA group and attenuated by C-PC treatment (Figure 4D; Supplementary Figure S3C, D). Mitochondrial bioenergetics were assessed via Seahorse XF analysis. Notably, C-PC markedly improved mitochondrial function (Figure 4E, F). The Mito Stress Test revealed significantly higher basal, maximal, and ATP-coupled mitochondrial oxygen consumption and glycolysis processes in DHEA-treated cells incubated with C-PC than in cells treated with DHEA alone (Figure 4E, F; Supplementary Figure S3E, F). Furthermore, C-PC improved cell viability, reduced LDH release, and suppressed Caspase-3 activity in C-PC-treated KGN cells, collectively indicating reduced apoptotic signaling (Supplementary Figure S3G–I). Overall, these findings demonstrate that C-PC increases cell viability by restoring mitochondrial function, reducing oxidative stress, and inhibiting ferroptosis in the context of DHEA-induced PCOS-

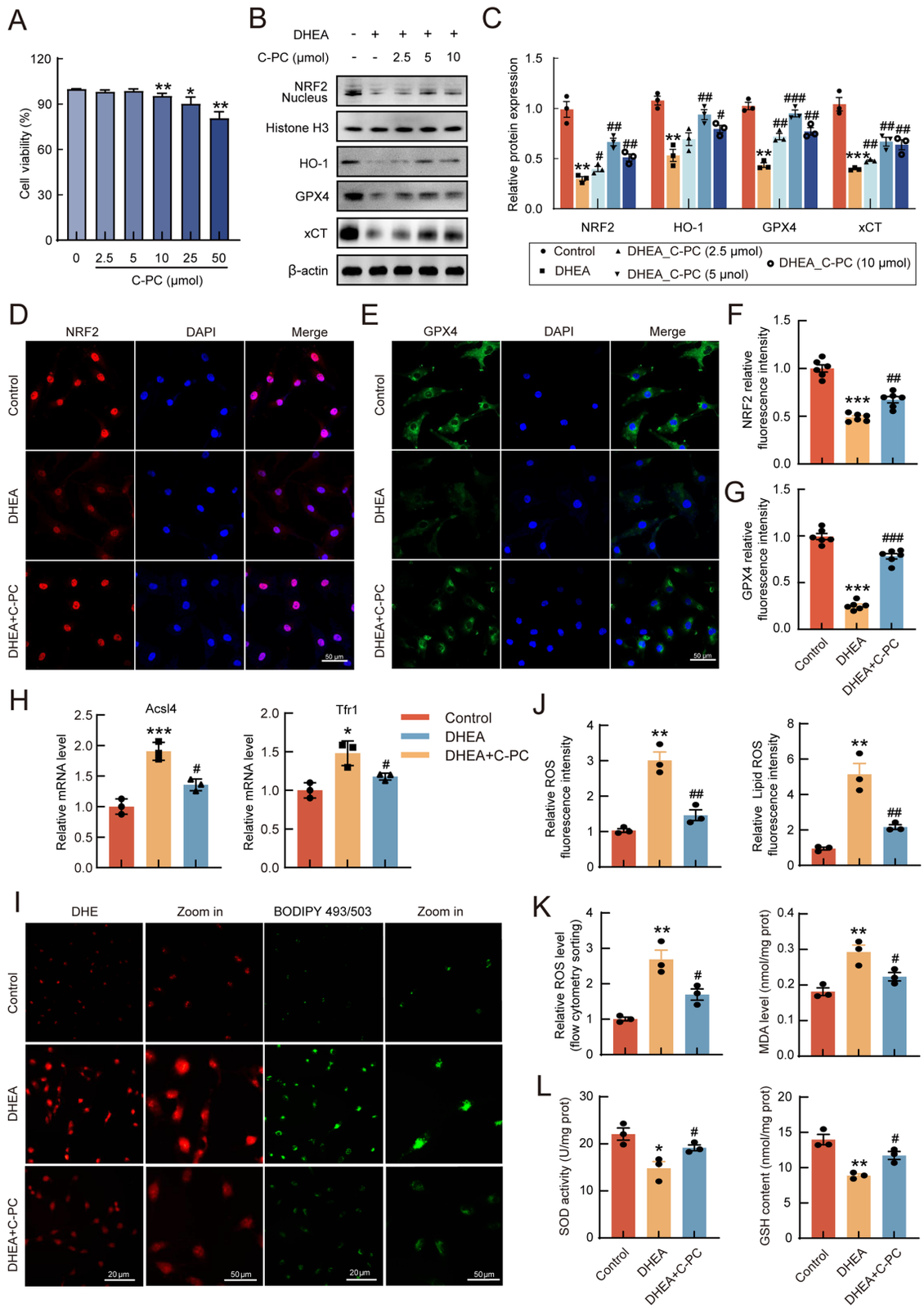


Figure 3 C-PC suppresses DHEA-induced ferroptosis in granulosa cells (GCs)

GCs were exposed to varying concentrations of C-PC. A: Cell viability following exposure to C-PC (0–50 μmol/L) (*n*=6). B, C: Total and nuclear GC lysates were extracted, and protein levels of HO-1, GPX4, xCT, and NRF2 were detected (*n*=3). D, E: Confocal fluorescent staining was used to evaluate NRF2 and GPX4 expression levels. F, G: Quantification of mean fluorescence intensity of NRF2 and GPX4 (*n*=6). H: Expression of genes related to ferroptosis (*ACSL4* and *TFR1*) determined by RT-qPCR (*n*=3). I: Intracellular reactive oxygen species (ROS) and lipid ROS levels visualized using dihydroethidium (DHE) and BODIPY 493/591 fluorescent probes, respectively. J: Quantification of ROS and lipid ROS fluorescence intensity (*n*=3). K: Intracellular ROS levels measured by flow cytometry (*n*=3). L: Levels of MDA, SOD, and GSH determined by ELISA (*n*=3). All experiments were independently repeated at least three times. Data are expressed as mean±SD. *: P<0.05; **: P<0.01; ***: P<0.001 vs. Control group; $^{\#}$: P<0.05; $^{\#\#}$: P<0.01; $^{\#\#\#}$: P<0.001 vs. DHEA group.

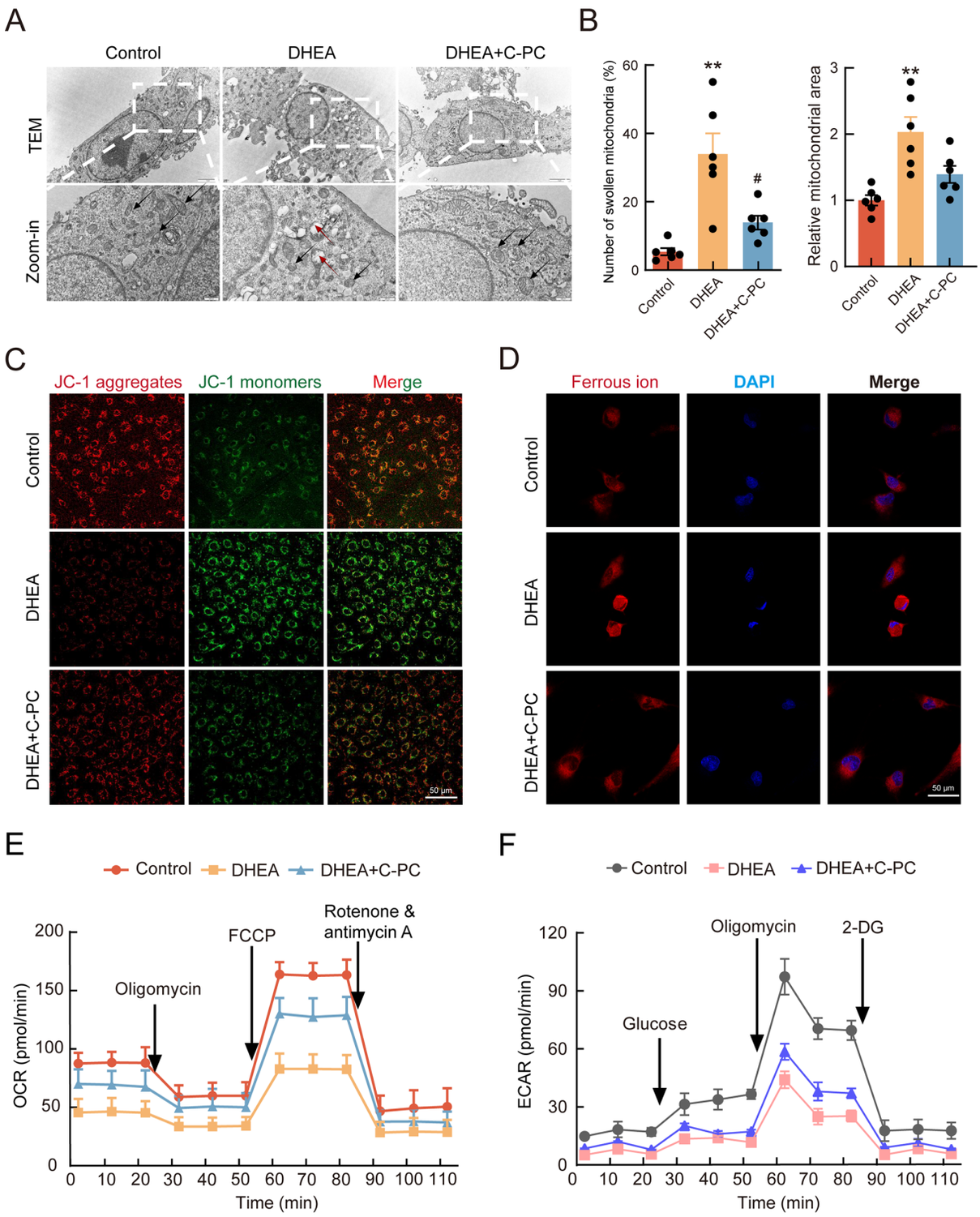


Figure 4 C-PC improves mitochondrial function in DHEA-induced GCs

GCs are pretreated with C-PC (5 μmol/L) for 2 h, followed by stimulation with 10 μmol/L DHEA. A, B: Representative transmission electron microscopy (TEM) images showing percentage of swollen mitochondria and relative mitochondrial area (n=6). C: Mitochondrial membrane potential (MMP) assessed by JC-1 staining. D: Ferrous ion (Fe^{2+}) levels evaluated by immunofluorescence staining using FerroOrange fluorescent probe. E, F: Mitochondrial function assessed using the Seahorse assay (n=12). Data are expressed as mean±SD. **: P<0.01 vs. Control group; #: P<0.05 vs. DHEA group.

related cellular injury.

C-PC inhibits ferroptosis in GCs by increasing antioxidant capacity

To further elucidate the mechanisms by which C-PC suppresses ferroptosis in DHEA-treated GCs, a series of pharmacological interventions and protein expression analyses were performed. Western blot analysis revealed that treatment with Fer-1 (10 μmol/L), a canonical ferroptosis inhibitor, elevated the protein expression of GPX4, xCT, and HO-1 while reducing levels of 4-HNE, a lipid peroxidation marker, suggesting that C-PC suppresses ferroptosis

(Figure 5A, B). To further delineate the role of iron-dependent oxidative injury, GCs were also treated with the iron chelator deferoxamine (DFO; 10 μmol/L). Results showed that C-PC mitigated lipid peroxidation and HO-1 levels, indicating that C-PC counteracts iron-catalyzed lipid damage and ferroptosis (Figure 5C, D). Given the established contribution of ROS to ferroptotic cell death, the modulatory effect of C-PC on ROS-associated signaling was assessed. GCs were pretreated with the antioxidant NAC or H_2O_2 for 1 h, followed by C-PC (5 μmol/L) administration and subsequent DHEA exposure (Figure 5E–H). NAC inhibited DHEA-induced expression of ferroptosis-related proteins GPX4, xCT, and HO-1, with C-PC shown to further suppress this expression, highlighting its antioxidant properties (Figure 5E, F). In contrast, H_2O_2 pretreatment amplified DHEA-induced ferroptosis-related protein expression, while co-treatment with C-PC markedly reduced these levels (Figure 5G, H). These findings demonstrate that C-PC mitigates ROS-induced ferroptosis in DHEA-stimulated GCs by enhancing antioxidant defense and limiting lipid peroxidation.

NRF2 is a key PCOS-related target of C-PC

To elucidate the regulatory mechanism by which C-PC inhibits NRF2 activation, a 50 ns molecular dynamics simulation was performed to assess the structural stability of the NRF2-C-PC complex. Hydrogen bond occupancy rapidly increased during the initial 20 ns and subsequently stabilized, indicating a stable binding interaction (Supplementary Figure S4A). Molecular docking further revealed strong affinity between C-PC and NRF2, with a calculated binding energy of –38.4 kcal/mol (Figure 6A). Mutational analysis and *in silico* prediction of critical residues confirmed that multiple hydrogen bonds contributed to reduced binding free energy, highlighting key amino acids mediating this interaction (Figure 6A). CETSA demonstrated a temperature-dependent increase in NRF2 protein stability following C-PC treatment, supporting direct binding of C-PC to NRF2 within the physiological range of 45–65°C (Figure 6B, C). These findings implicate NRF2 as a principal molecular target through which C-PC exerts protective effects in PCOS.

Previous research has shown that NRF2 regulates the transcription of antioxidant and ferroptosis-inhibitory genes, including GPX4 and xCT (50, 51). Thus, we speculated that C-PC may activate the NRF2 pathway to increase GPX4 and xCT expression in GCs. ChIP-qPCR analysis revealed significantly increased enrichment of NRF2 on the promoter regions of both GPX4 and xCT following C-PC treatment compared to the DHEA group (Figure 6D), indicating direct transcriptional activation. Given our previous results suggesting that C-PC reduces oxidative stress by activating NRF2 (Figure 3), whether NRF2 signaling mediates the anti-ferroptotic effects of C-PC was further explored. GCs were pretreated with selective NRF2 inhibitor ML385 (5 μmol/L) prior to C-PC exposure. Results showed that ML385 abrogated the C-PC-induced up-regulation of xCT and GPX4 (Figure 6D, E; Supplementary Figure S4B–F). Immunofluorescence analysis revealed that NRF2 inhibition reversed C-PC-mediated protection, as shown by diminished GPX4 expression and elevated levels of ROS and lipid ROS (Figure 6F, G; Supplementary Figure S4G–I). These results confirm that C-PC inhibits GC ferroptosis by activating the NRF2-dependent antioxidant pathways in GCs.

To validate the essential role of NRF2 in mediating C-PC function, NRF2 expression was silenced *in vitro* using shRNA constructs. RT-qPCR analysis indicated that sh-NRF2 reduced NRF2 expression by approximately 70%, indicating effective gene silencing (Supplementary Figure S5A). *In vivo*, AAV-sh-NRF2 or AAV-sh-NC was administered via tail vein injection in PCOS model mice (Figure 7A). Mice receiving AAV-sh-NC and treated with C-PC exhibited elevated expression of oxidative stress- and ferroptosis-related proteins (NRF2, HO-1, GPX4 and xCT; Figure 7B; Supplementary Figure S5B, C), along with a significant reduction in cystic follicle formation, as shown by H&E staining (Figure 7C). Conversely, the AAV-sh-NRF2-injected mice exhibited a decrease in NRF2 expression and down-regulation of GPX4 and xCT, as indicated by immunofluorescence staining. RT-qPCR analysis confirmed a significant decrease in the expression of other ferroptosis-related markers, including *ACSL4* and *TFR1* (Figure 7D, E; Supplementary Figure S5D, E). Endocrine analysis further indicated that NRF2 silencing reversed the C-PC-mediated normalization of serum T, E2, P4, and the LH/FSH ratio (Figure 7F; Supplementary Figure S5F). Oxidative stress markers were also affected by NRF2 silencing. C-PC treatment significantly increased serum levels of SOD, GSH, and CAT, while reducing MDA, consistent with enhanced antioxidant defense. These improvements were abolished by NRF2 knockdown, indicating that the redox-restorative effects of C-PC are mediated via NRF2 activation (Figure 7G). Collectively, these findings establish NRF2 as a direct molecular target of C-PC and demonstrate that NRF2 signaling is essential for the suppression of ferroptosis and restoration of ovarian function in PCOS.

C-PC inhibits ferroptosis via the ROS/AMPK pathway

Western blot analysis demonstrated that C-PC markedly reduced AMPK phosphorylation in GCs (Figure 8A, B). To determine whether C-PC-mediated inhibition of ferroptosis was dependent on AMPK signaling, the potent AMPK activator AICAR was employed as a positive control (Figure 8C). AICAR exposure reversed the upregulation of GPX4 and xCT induced by C-PC, indicating that AMPK activation counteracted the ferroptosis-inhibitory effects of C-PC (Figure 8D, E). Further analysis showed that pretreatment with NAC, an antioxidant, mimicked the suppressive effect of C-PC on AMPK phosphorylation, suggesting that C-PC modulates AMPK activity in a ROS-dependent manner. Notably, combined treatment with NAC and C-PC did not produce an additive effect (Figure 8F, G). These results suggest that C-PC inhibits ferroptosis by activating the ROS/AMPK signaling pathway.

DISCUSSION

PCOS, affecting approximately 5%–10% of reproductive-aged women, involves complex endocrine, metabolic, and psychological disturbances. Oxidative stress is now recognized as a critical factor in PCOS pathophysiology, yet the mechanistic links between redox imbalance and GC dysfunction remain incompletely defined. Intracellular ROS production and accumulation are controlled by highly complex antioxidant enzymatic and nonenzymatic systems, understanding the mechanisms by which oxidative stress occurs is important for developing strategies for the prevention and treatment of PCOS. Although cells are equipped with intricate enzymatic and non-enzymatic antioxidant systems to maintain redox homeostasis, persistent elevations in ROS

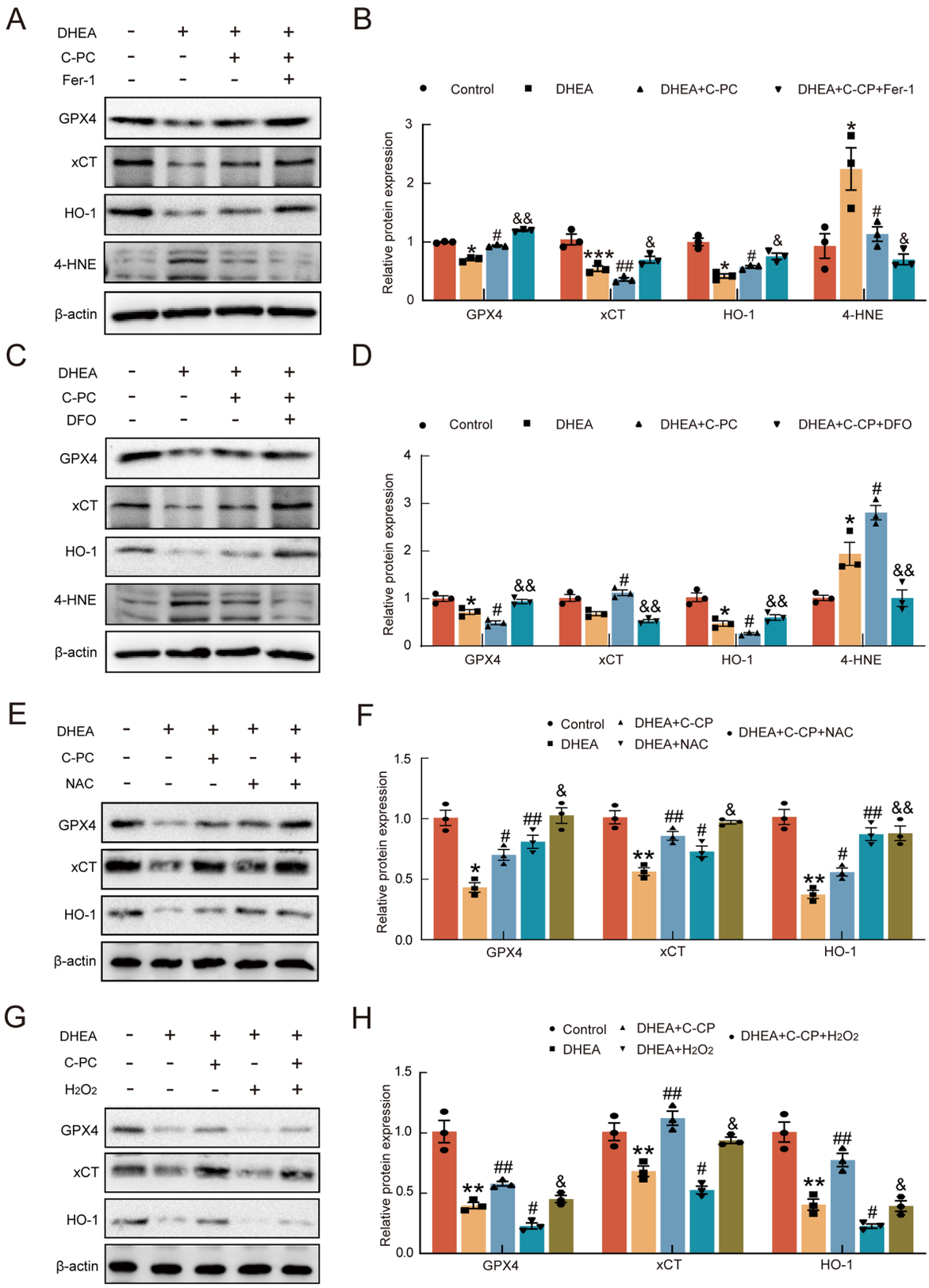


Figure 5 C-PC inhibits ferroptosis by modulating oxidative stress in DHEA-treated GCs

A–D: GCs were preincubated with either ferrostatin-1 (Fer-1), a ferroptosis inhibitor (A, B), or deferoxamine (DFO), an iron chelator, for 1 h prior to supplementation with C-PC (2 h) and subsequent exposure to DHEA (10 μmol/L, 48 h) in DMEM. (C, D) Expression levels of GPX4, xCT, HO-1, and 4-HNE in GCs were analyzed by western blotting and quantified. E–H: Effects of N-acetylcysteine (NAC) and H_2O_2 on DHEA-induced ferroptosis-related protein expression (E, G). Expression levels of GPX4, xCT, HO-1, and 4-HNE in GCs were analyzed using western blotting and quantified (F, H) (n=3). Data are expressed as mean±SD. *: P<0.05; **: P<0.01; ***: P<0.001 vs. Control group; $^{\#}$: P<0.05; $^{\#\#}$: P<0.01; $^{\#\#\#}$: P<0.001 vs. DHEA group; $^{\&}$: P<0.05 ; $^{\&\&}$: P<0.01 vs. DHEA+Fer-1/DFO/NAC/H_2O_2 group.

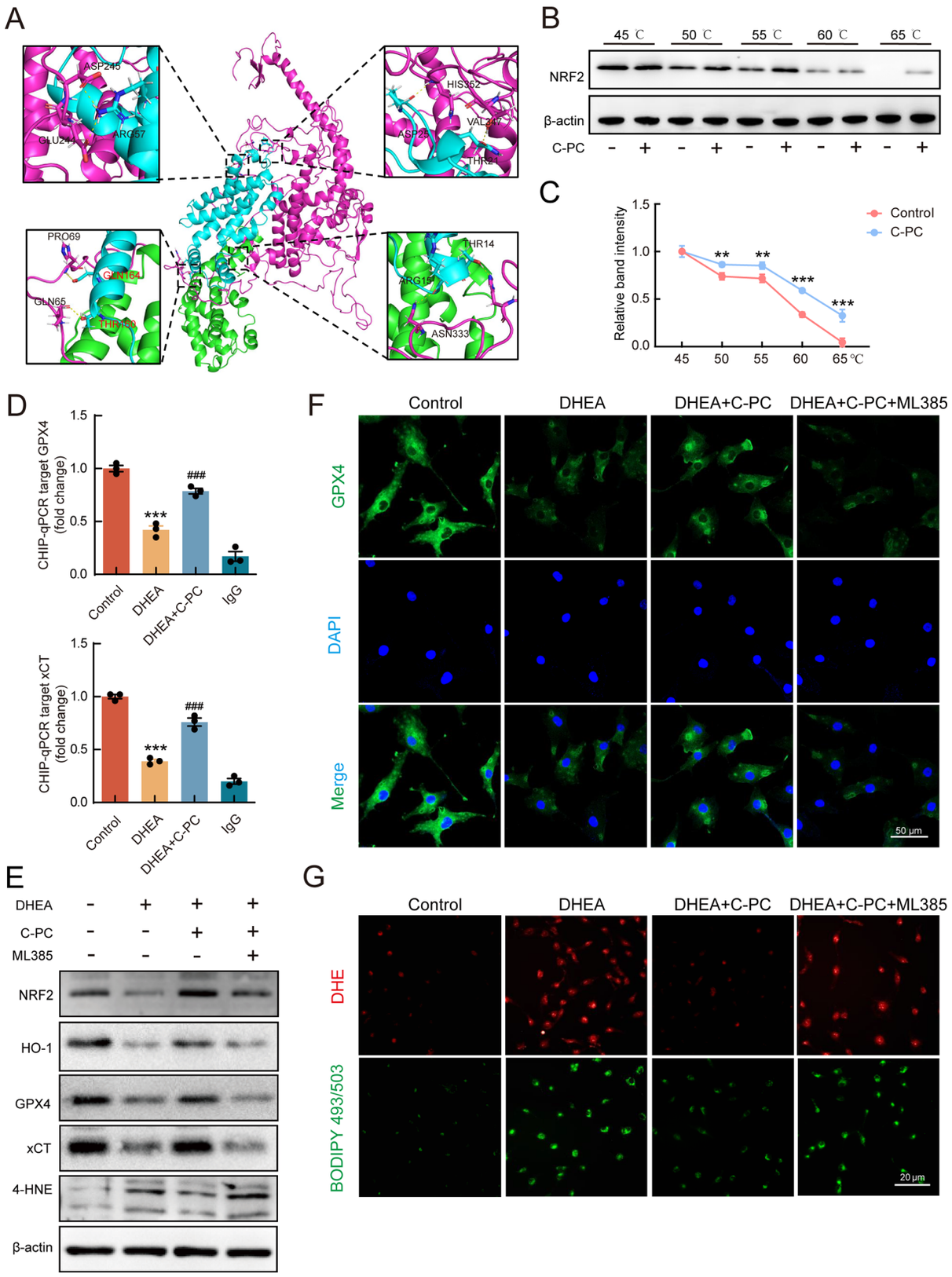


Figure 6 NRF2 is a predicted key target of C-PC in ferroptosis regulation relevant to PCOS treatment

A: Molecular docking model showing interaction between C-PC and NRF2 protein. B: Protein stability of NRF2 assessed by CETSA. C: NRF2 protein expression in GCs. D: ChIP-qPCR analysis of NRF2 enrichment on GPX4 and xCT promoter regions (n=3). GCs were preincubated with C-PC (5 μmol/L, 2 h) prior to supplementation with ML385 (5 μmol/L, 1 h) and subsequent exposure to DHEA (10 μmol/L, 48 h) in DMEM. E: Western blotting was performed to assess expression levels of NRF2, HO-1, GPX4, xCT, and 4-HNE in GCs. F: Immunofluorescence images of GPX4 expression. Sca$le bar: 50 μm. G: Intracellular ROS and lipid ROS visualized using DHE and BODIPY 493/591 fluorescent probes, respectively. Scale bar: 20 μm. Values are expressed as mean±SD. ***: P<0.001 vs. Control group; $^{###}$: P<0.001 vs. DHEA group.

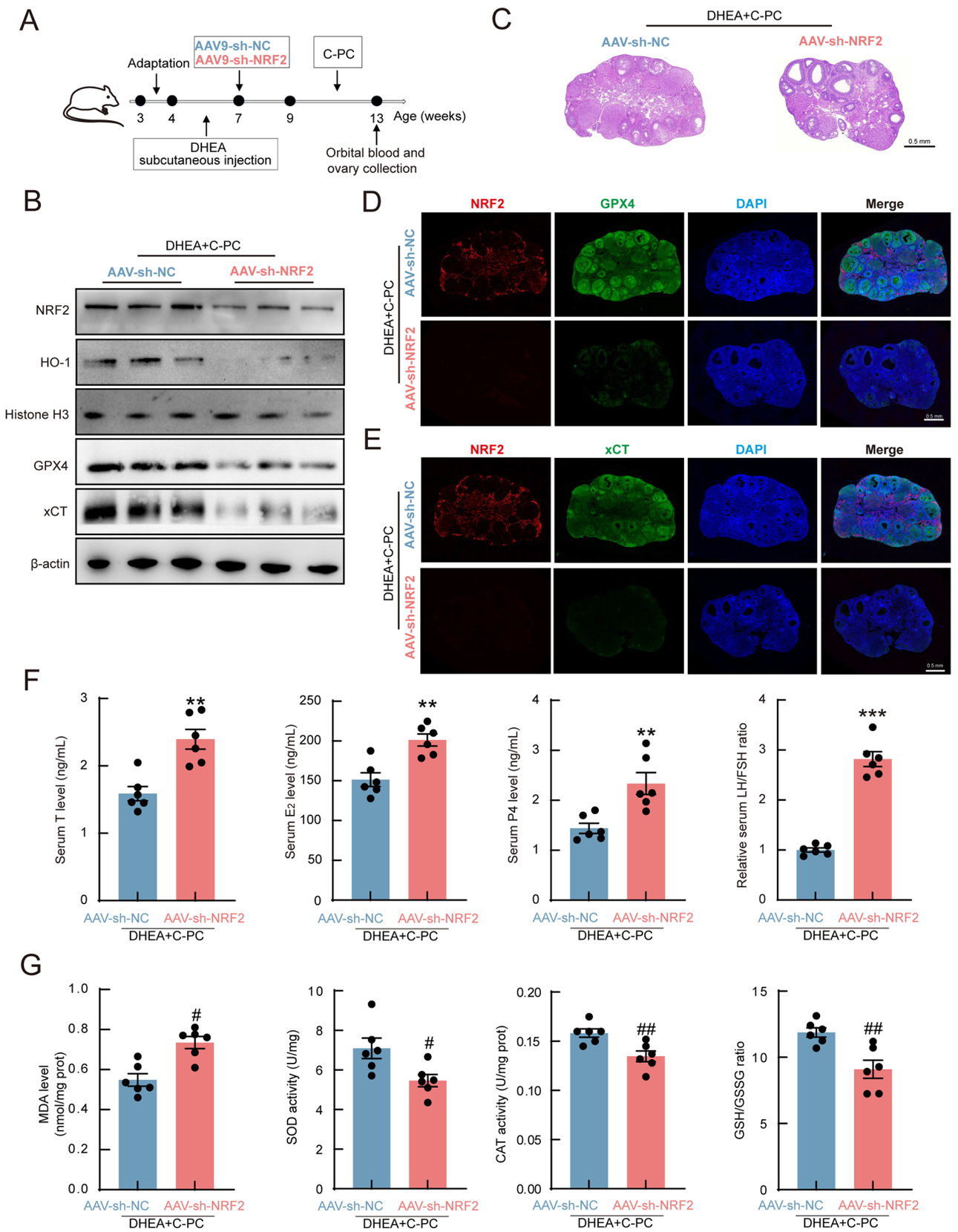


Figure 7 AAV-shNRF2 abrogates the therapeutic effects of C-PC in PCOS model mice

A: Schematic overview of AAV-shNRF2 experiment. PCOS mice (7 weeks old) were injected with AAV9-shNRF2 or AAV9-sh-NC (negative control), followed by C-PC treatment initiated 4 weeks post-injection. B: Ovarian expression of NRF2, GPX4, and xCT proteins evaluated by western blotting (n=3). C: Representative H&E-stained ovarian sections. D, E: Immunofluorescence staining of NRF2/GPX4 or NRF2/xCT in ovarian tissues. F: Effects of C-PC on serum T, E2, P4, and LH/FSH ratio (n=6). G: Ovarian oxidative stress markers, including MDA, SOD, CAT, and GSH/GSSG, determined by ELISA (n=6). Three independent experiments were performed with similar results. Data are expressed as mean±SD. *: P<0.05; **: P<0.01; ***: P<0.001 vs. AVV9-sh-NC group.

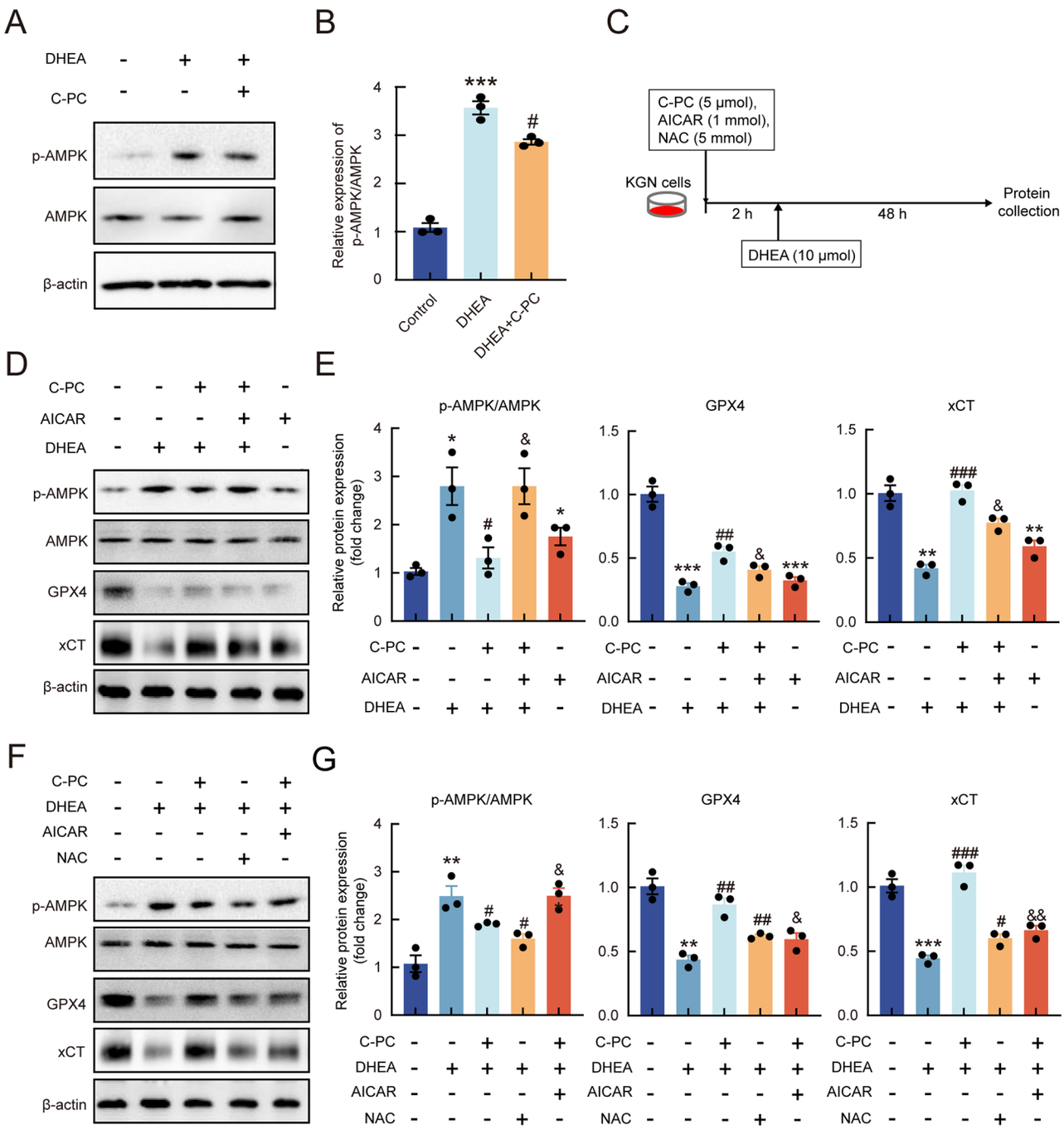


Figure 8 C-PC suppresses ferroptosis in GCs partly via the ROS/AMPK signaling pathway

A: Western blot analysis of phosphorylated AMPK (p-AMPK) and total AMPK in GCs treated with DHEA. B: Quantification of p-AMPK/AMPK protein levels using ImageJ (n=3). C: Experimental study layout. KGN cells were pretreated with C-PC (5 μmol/L), AICAR (1 mmol/L, specific AMPK activator), or NAC (5 mmol/L) for 2 h, then stimulated with 10 μmol/L DHEA for 48 h. D–G: Western blot analysis of p-AMPK/AMPK, GPX4, and xCT expression levels and quantification using ImageJ software (n=3). Data are expressed as mean±SD. *: P<0.05; **: P<0.01; ***: P<0.001 vs. Control group; $^{\#}$: P<0.05; $^{\#\#}$: P<0.01; $^{\#\#\#}$: P<0.001 vs. DHEA group; $^{\&}$: P<0.05 vs. DHEA+C-PC group.

contribute to cellular injury and disease progression. Defining the mechanisms that govern oxidative damage in PCOS is essential for the development of targeted interventions.

This study demonstrated that C-PC, a biliprotein derived from cyanobacteria, protects GCs against ferroptosis, a form of regulated cell death driven by iron-dependent lipid peroxidation and implicated in PCOS-related follicular atresia. C-PC suppressed intracellular ROS accumulation, attenuated lipid peroxidation, and up-regulated ferroptosis defense proteins GPX4 and xCT in a dose-dependent manner. Mechanistically, C-PC activated NRF2 signaling and modulated ROS/AMPK dynamics to restore redox equilibrium. Notably, these findings uncover a previously unrecognized antioxidant role of C-PC and suggest its therapeutic potential in PCOS (Figure 9).

C-PC has been extensively characterized for its pharmacological effects, including ROS-scavenging activities (Bhat & Madyastha, 2000) and antioxidant (Bhat & Madyastha, 2000), hepatoprotective (Vadiraja et al., 1998), and anti-arthritic properties (González et al., 1999). Supporting

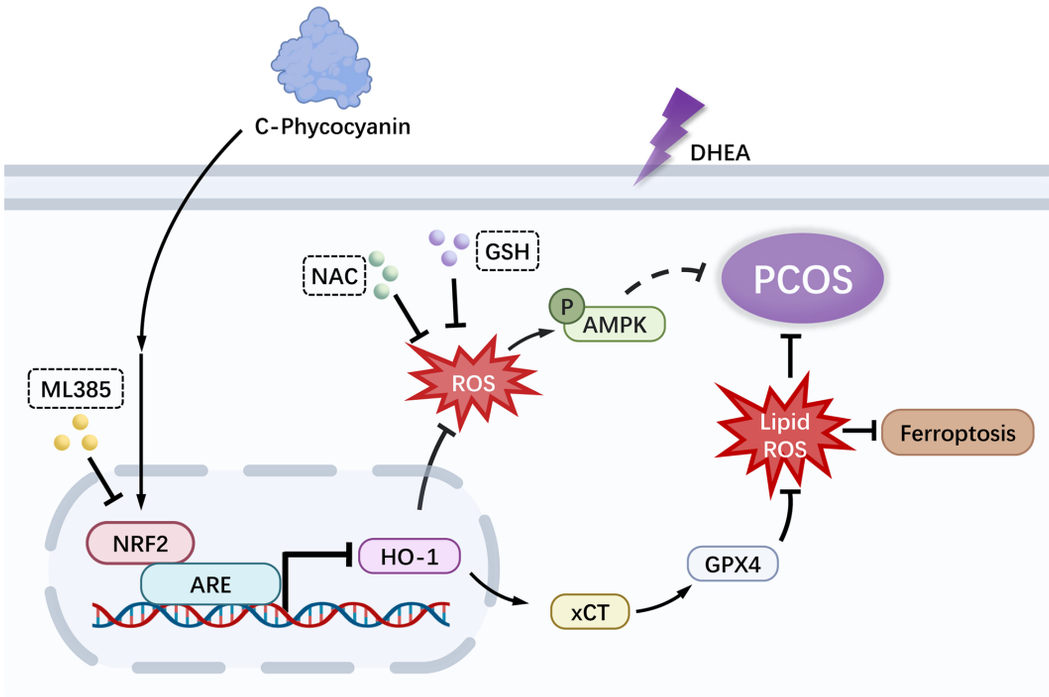


Figure 9 Schematic overview of mechanisms by which C-PC mediates anti-ferroptotic activity

this, the present study demonstrated that C-PC significantly attenuated DHEA-induced ROS generation both *in vitro* and *in vivo*. Administration of NAC and H_2O_2 reduced ROS levels in GCs and partially abrogated the inhibitory effects of C-PC on xCT and GPX4 expression and ROS production. In the context of PCOS, excessive ROS has been shown to impair GC viability and contribute to follicular degeneration. In the current study, ROS acted as a critical upstream trigger of ferroptosis by promoting lipid peroxidation and impairing the NRF2/xCT/GPX4 antioxidant defense system. Of note, C-PC alleviated oxidative stress and inhibited ferroptosis in GCs by activating NRF2 signaling. Furthermore, ROS-induced activation of AMPK appeared to suppress NRF2-mediated protection, with AMPK activation shown to reverse the effects of C-PC on GPX4 and xCT expression. Collectively, these findings highlight the pivotal role of the ROS-ferroptosis axis in PCOS pathogenesis and establish C-PC as a potential therapeutic agent restoring redox homeostasis and preventing ferroptosis-mediated follicular damage in PCOS.

NRF2 functions as a master regulator of cellular redox homeostasis, orchestrating a broad transcriptional response to oxidative stress through modulation of GSH synthesis, iron metabolism, lipid peroxidation, and mitochondrial function (Abdalkader et al., 2018; La Rosa et al., 2021). Although activation of NRF2 signaling has been implicated in cancer progression by enhancing resistance to ferroptosis inducers (Dong et al., 2020), NRF2 remains a critical transcriptional factor for maintaining redox balance in non-malignant contexts. Given its established roles in regulating xCT and GPX4 expression, NRF2 was investigated as a potential target of C-PC, a well-characterized ROS scavenger (Bhat & Madyastha, 2000). Molecular docking analysis predicted a specific binding interface between C-PC and NRF2, suggesting that C-PC may modulate NRF2 activity directly. Functional validation showed that C-PC treatment increased xCT and GPX4 protein levels both *in vitro* and in PCOS model mice. Pharmacological inhibition of NRF2 with ML385 (5 μmol/L) in GCs, as well as *in vivo* knockdown using AAV-shNRF2, abrogated these effects. In addition, downstream modulation of MDA levels confirmed activation of NRF2 signaling by C-PC. These results establish NRF2 as a key mediator of C-PC-induced ferroptosis resistance in GCs through activation of the NRF2-GPX4 antioxidant axis.

Previous evidence supports the role of NRF2 signaling in mediating the therapeutic and biological effects of C-PC across multiple disease contexts (Dong et al., 2022). Antioxidant peptides derived from C-PC have been reported to mitigate UVB-induced apoptosis in human skin cells through a PKC α/βII-Nrf-2/HO-1-dependent pathway (Kim et al., 2018), and to attenuate acute myocardial infarction-induced oxidative stress, inflammation, and cardiac damage (Blas-Valdivia et al., 2022). The current findings expand this understanding by demonstrating that C-PC modulates NRF2-dependent ferroptosis resistance in GCs, thereby providing a mechanistic basis for its potential therapeutic application in PCOS. Nonetheless, further studies are warranted to dissect upstream regulators and downstream effectors of this pathway and to explore potential crosstalk with other ferroptosis-relevant networks.

Several study limitations should be acknowledged. First, analyses of ferroptosis and DHEA-related factors were conducted in an established GC line rather than in primary GCs isolated directly from PCOS model ovaries. This limits the physiological relevance of the findings, as *in vivo* validation in primary cells would provide more robust evidence. Additionally, although C-PC demonstrated potent ferroptosis-inhibitory activity, its specific effects within the ovarian microenvironment of PCOS remain insufficiently characterized. Consequently, the temporal relationship between ferroptosis and inflammatory responses also remains unresolved, and the potential existence of reciprocal regulation between these processes was not investigated. The selected C-PC dose was based on prior murine studies showing efficacy without toxicity. Although C-PC is widely

recognized as a safe, food-grade antioxidant, further research is needed to determine its optimal dose and safety profile in humans.

Future investigations should evaluate whether C-PC influences other cell death modalities, including apoptosis and autophagy, and include appropriate inhibitor-only control groups to strengthen causal inferences regarding ferroptosis suppression. Furthermore, while DHEA-induced ferroptosis may activate innate immune pathways and promote inflammatory cytokine release and inflammation, interactions between immune signaling and ferroptotic cell death require further elucidation. Although our study supported NRF2-mediated regulation of xCT and GPX4, further research is needed to investigate the underlying mechanisms of ferroptosis-related iron metabolism and other processes in GCs. The absence of NRF2 expression data from ovarian tissues of PCOS patients also limits the translational relevance of the findings. Inclusion of such clinical samples in future studies would enhance the applicability of the results.

Furthermore, this study did not include other established antioxidants such as N-acetylcysteine or vitamin E, which could serve as comparators to determine whether C-PC confers distinct mechanistic or therapeutic benefits. Although C-PC was shown to activate NRF2 signaling, the precise molecular mechanisms underlying this activation remain to be fully elucidated. Previous work has shown that monomeric compounds and proteins can activate NRF2 by competitively binding to KEAP1, thereby disrupting the KEAP1-NRF2 complex and promoting NRF2 expression (He et al., 2023; Luo et al., 2022, 2024; Wang et al., 2024a). Whether C-PC exerts similar effects through direct interaction with KEAP1 remains unknown. Therefore, future studies employing molecular docking, structural analysis, and site-directed mutagenesis will be essential to identify direct binding targets and interaction modes between C-PC and KEAP1 or NRF2. Such mechanistic insights would significantly strengthen the evidence establishing a definitive link between C-PC and NRF2 pathway modulation. Moreover, additional *in vivo* studies are required to validate these molecular interactions and confirm their physiological relevance.

Finally, it should be noted that the DHEA-induced PCOS mouse model primarily recapitulates estrous cycle irregularities and does not fully mimic all clinical diagnostic features of human PCOS, such as hyperandrogenism and polycystic ovarian morphology as defined by the Rotterdam criteria. This limitation may constrain the direct translational applicability of the findings. Future studies utilizing alternative or complementary models that more comprehensively reflect the human pathophysiological spectrum of PCOS are warranted.

CONCLUSION

This study showed that C-PC mitigated DHEA-induced oxidative damage in GCs by reducing intracellular ROS and lipid peroxidation and suppressing ferroptotic cell death. Furthermore, C-PC alleviated pathological processes in PCOS model mice by inhibiting GC ferroptosis, at least in part through activation of the NRF2 and ROS/AMPK signaling pathways and modulation of GPX4/xCT expression. Further investigation is required to evaluate optimal administration methods, potential risks, and the comparative efficacy of alternative ferroptosis inhibitors. Moreover, as this is a preliminary study, additional research is needed to validate these results and clarify the broader therapeutic potential of C-PC in the context of PCOS.

SUPPLEMENTARY DATA

Supplementary data to this article can be found online.

COMPETING INTERESTS

The authors declare that they have no competing interests.

AUTHORS' CONTRIBUTIONS

All authors contributed to study conception and design. J.Z., Conceptualization, Methodology, Data curation, Writing – original draft. Q.S.S. and Y.X.C., Methodology, Data curation, Software, Writing – original draft, Visualization, Investigation. H.R.C., W.Z., T.X., and Y.J.L., Methodology, Software, Data curation, Validation. Y.X.C., M.L., and D.L., Methodology, Software, Data curation, Supervision, Validation, Writing – review & editing. B.Y., Data curation, Supervision, Validation, Writing – review & editing. All authors read and approved the final version of the manuscript.

ACKNOWLEDGMENTS

We thank the NHC Key Laboratory of Study on Abnormal Gametes and Reproductive Tract, Anhui Medical University, for the support of this research project. We also thank Cheng-Yu Zhang for cartoon illustrations and experimental assistance.

REFERENCES

Abdalkader M, Lampinen R, Kanninen KM, et al. 2018. Targeting Nrf2 to suppress ferroptosis and mitochondrial dysfunction in neurodegeneration. *Frontiers in Neuroscience*, **12**: 466.

Agarwal A, Aponte-Mellado A, Premkumar BJ, et al. 2012. The effects of oxidative stress on female reproduction: a review. *Reproductive Biology and Endocrinology*, **10**: 49.

Amin AF, Abd El-Aal DEM, Darwish AM, et al. 2003. Evaluation of the impact of laparoscopic ovarian drilling on Doppler indices of ovarian stromal blood flow, serum vascular endothelial growth factor, and insulin-like growth factor-1 in women with polycystic ovary syndrome. *Fertility and Sterility*, **79**(4): 938–941.

Ananth S, Miyauchi S, Thangaraju M, et al. 2021. Selenomethionine (Se-Met) induces the cystine/glutamate exchanger SLC7A11 in cultured human retinal pigment epithelial (RPE) cells: implications for antioxidant therapy in aging retina. *Antioxidants*, **10**(1): 9.

Azziz R, Woods KS, Reyna R, et al. 2004. The prevalence and features of the polycystic ovary syndrome in an unselected population. *The Journal of Clinical Endocrinology & Metabolism*, **89**(6): 2745–2749.

Barlow KA, Conchúir SÓ, Thompson S, et al. 2018. Flex ddG: rosetta ensemble-based estimation of changes in protein-protein binding affinity upon mutation. *The Journal of Physical Chemistry B*, **122**(21): 5389–5399.

Bersuker K, Hendricks JM, Li ZP, et al. 2019. The CoQ oxidoreductase FSP1 acts parallel to GPX4 to inhibit ferroptosis. *Nature*, **575**(7784): 688–692.

Bhat VB, Madyastha KM. 2000. C-phycocyanin: a potent peroxyl radical scavenger *in vivo* and *in vitro*. *Biochemical and Biophysical Research Communications*, **275**(1): 20–25.

Blas-Valdivia V, Moran-Dorantes DN, Rojas-Franco P, et al. 2022. C-Phycocyanin prevents acute myocardial infarction-induced oxidative stress, inflammation and cardiac damage. *Pharmaceutical Biology*, **60**(1): 755–763.

Chen ZK, Xie JT, Ma CY, et al. 2025. Oxidative damage under microgravity conditions: response mechanisms, monitoring methods and countermeasures on somatic and germ cells. *International Journal of Molecular Sciences*, **26**(10): 4583.

Dodson M, Castro-Portuguez R, Zhang DD. 2019. NRF2 plays a critical role

in mitigating lipid peroxidation and ferroptosis. *Redox Biology*, **23**: 101107.

Dong H, Qiang ZZ, Chai DD, et al. 2020. Nrf2 inhibits ferroptosis and protects against acute lung injury due to intestinal ischemia reperfusion via regulating SLC7A11 and HO-1. *Aging*, **12**(13): 12943–12959.

Dong XL, Yang FH, Xu XH, et al. 2022. Protective effect of C-phycocyanin and apo-phycocyanin subunit on programmed necrosis of GC-1 spg cells induced by H_2O_2. *Environmental Toxicology*, **37**(6): 1275–1287.

González R, Rodríguez S, Romay C, et al. 1999. Anti-inflammatory activity of phycocyanin extract in acetic acid-induced colitis in rats. *Pharmacological Research*, **39**(1): 1055–1059.

Goodarzi MO, Dumesic DA, Chazenbalk G, et al. 2011. Polycystic ovary syndrome: etiology, pathogenesis and diagnosis. *Nature Reviews Endocrinology*, **7**(4): 219–231.

Goud AP, Goud PT, Diamond MP, et al. 2008. Reactive oxygen species and oocyte aging: role of superoxide, hydrogen peroxide, and hypochlorous acid. *Free Radical Biology and Medicine*, **44**(7): 1295–1304.

He XY, Zhou YB, Chen WJ, et al. 2023. Repurposed pizotifen malate targeting NRF2 exhibits anti-tumor activity through inducing ferroptosis in esophageal squamous cell carcinoma. *Oncogene*, **42**(15): 1209–1223.

Huang JC, Duan CC, Jin S, et al. 2022. HB-EGF induces mitochondrial dysfunction via estrogen hypersecretion in granulosa cells dependent on cAMP-PKA-JNK/ERK-Ca^{2+}-FOXO1 pathway. *International Journal of Biological Sciences*, **18**(5): 2047–2059.

Huang JY, Zhao J, Geng XY, et al. 2021. Long non-coding RNA lnc-CCNL1–3: 1 promotes granulosa cell apoptosis and suppresses glucose uptake in women with polycystic ovary syndrome. *Molecular Therapy Nucleic Acids*, **23**: 614–628.

Igbo EJ, Okoliko U, Aminu I, et al. 2022. Structural changes in the medial prefrontal cortex and anterior cingulate cortex of dehydroepiandrosterone-induced wistar rat model of polycystic ovarian syndrome. *Basic and Clinical Neuroscience*, **13**(5): 695–708.

Irato P, Santovito G. 2021. Enzymatic and non-enzymatic molecules with antioxidant function. *Antioxidants*, **10**(4): 579.

Khadrawy O, Gebremedhn S, Salilew-Wondim D, et al. 2019. Endogenous and exogenous modulation of Nrf2 mediated oxidative stress response in bovine granulosa cells: potential implication for ovarian function. *International Journal of Molecular Sciences*, **20**(7): 1635.

Kim KM, Lee JY, Im AR, et al. 2018. Phycocyanin protects against UVB-induced apoptosis through the PKC α/βII-Nrf-2/HO-1 dependent pathway in human primary skin cells. *Molecules*, **23**(2): 478.

Kuddus M, Singh P, Thomas G, et al. 2013. Recent developments in production and biotechnological applications of C-phycocyanin. *BioMed Research International*, **2013**: 742859.

La Rosa P, Petrillo S, Turchi R, et al. 2021. The Nrf2 induction prevents ferroptosis in Friedreich's Ataxia. *Redox Biology*, **38**: 101791.

Li B, Chu XM, Xu YJ, et al. 2013. CD59 underlines the antiatherosclerotic effects of C-phycocyanin on mice. *BioMed Research International*, **2013**: 729413.

Li J, Cao F, Yin HL, et al. 2020. Ferroptosis: past, present and future. *Cell Death & Disease*, **11**(2): 88.

Li XX, Qi J, Zhu QL, et al. 2019. The role of androgen in autophagy of granulosa cells from PCOS. *Gynecological Endocrinology*, **35**(8): 669–672.

Li XY, Lin YY, Cheng XY, et al. 2024a. Ovarian ferroptosis induced by androgen is involved in pathogenesis of PCOS. *Human Reproduction Open*, **2024**(2): hoae013.

Li YY, Peng YQ, Yang YX, et al. 2024b. Baicalein improves the symptoms of polycystic ovary syndrome by mitigating oxidative stress and ferroptosis in the ovary and gravid placenta. *Phytomedicine*, **128**: 155423.

Liu SH, Navarro G, Mauvais-Jarvis F. 2010. Androgen excess produces systemic oxidative stress and predisposes to β-cell failure in female mice. *PLoS One*, **5**(6): e11302.

Lu JY, Wang ZX, Cao J, et al. 2018. A novel and compact review on the role of oxidative stress in female reproduction. *Reproductive Biology and Endocrinology*, **16**(1): 80.

Luo M, Huang JC, Yang ZQ, et al. 2020a. Hydroxysafflor yellow A exerts beneficial effects by restoring hormone secretion and alleviating oxidative stress in polycystic ovary syndrome mice. *Experimental Physiology*, **105**(2): 282–292.

Luo M, Yang ZQ, Huang JC, et al. 2020b. Genistein protects ovarian granulosa cells from oxidative stress via cAMP-PKA signaling. *Cell Biology International*, **44**(2): 433–445.

Luo M, Zheng LW, Wang YS, et al. 2021. Genistein exhibits therapeutic potential for PCOS mice *via* the ER-Nrf2-Foxo1-ROS pathway. *Food & Function*, **12**(18): 8800–8811.

Luo X, Wang YH, Zhu XX, et al. 2024. MCL attenuates atherosclerosis by suppressing macrophage ferroptosis via targeting KEAP1/NRF2 interaction. *Redox Biology*, **69**: 102987.

Luo X, Weng XZ, Bao XY, et al. 2022. A novel anti-atherosclerotic mechanism of quercetin: competitive binding to KEAP1 via Arg483 to inhibit macrophage pyroptosis. *Redox Biology*, **57**: 102511.

Ma HD, Wang XD, Zhang WL, et al. 2020. Melatonin suppresses ferroptosis induced by high glucose via activation of the Nrf2/HO-1 signaling pathway in type 2 diabetic osteoporosis. *Oxidative Medicine and Cellular Longevity*, **2020**: 9067610.

Merhi Z, Kandaraki EA, Diamanti-Kandarakis E. 2019. Implications and future perspectives of AGEs in PCOS pathophysiology. *Trends in Endocrinology & Metabolism*, **30**(3): 150–162.

Narayanan C, Dias CL. 2013. Hydrophobic interactions and hydrogen bonds in β-sheet formation. *The Journal of Chemical Physics*, **139**(11): 115103.

Ou Y, Lin L, Pan Q, et al. 2012. Preventive effect of phycocyanin from *Spirulina platensis* on alloxan-injured mice. *Environmental Toxicology and Pharmacology*, **34**(3): 721–726.

Pan X, Liu YF, Liu LQ, et al. 2022. Bushen Jieyu Tiaochong Formula reduces apoptosis of granulosa cells via the PERK-ATF4-CHOP signaling pathway in a rat model of polycystic ovary syndrome with chronic stress. *Journal of Ethnopharmacology*, **292**: 114923.

Papalou O, Victor VM, Diamanti-Kandarakis E. 2016. Oxidative stress in polycystic ovary syndrome. *Current Pharmaceutical Design*, **22**(18): 2709–2722.

Patil G, Chethana S, Sridevi AS, et al. 2006. Method to obtain C-phycocyanin of high purity. *Journal of Chromatography A*, **1127**(1-2): 76–81.

Piovan A, Filippini R, Argentini C, et al. 2022. The effect of C-phycocyanin on microglia activation is mediated by toll-like receptor 4. *International Journal of Molecular Sciences*, **23**(3): 1440.

Reddy CM, Bhat VB, Kiranmai G, et al. 2000. Selective inhibition of cyclooxygenase-2 by C-phycocyanin, a biliprotein from *Spirulina platensis*. *Biochemical and Biophysical Research Communications*, **277**(3): 599–603.

Romay C, Gonzalez R, Ledon N, et al. 2003. C-phycocyanin: a biliprotein with antioxidant, anti-inflammatory and neuroprotective effects. *Current Protein & Peptide Science*, **4**(3): 207–216.

Roy KR, Arunasree KM, Reddy NP, et al. 2007. Alteration of mitochondrial membrane potential by Spirulina platensis C-phycocyanin induces apoptosis in the doxorubicinresistant human hepatocellular-carcinoma cell line HepG2. *Biotechnology and Applied Biochemistry*, **47**(Pt 3): 159–167.

Rzońca E, Bień A, Wdowiak A, et al. 2018. Determinants of quality of life and satisfaction with life in women with polycystic ovary syndrome. *International Journal of Environmental Research and Public Health*, **15**(2): 376.

Sadeghi HM, Adeli I, Calina D, et al. 2022. Polycystic ovary syndrome: a comprehensive review of pathogenesis, management, and drug

repurposing. *International Journal of Molecular Sciences*, **23**(2): 583.
Schiffrin B, Radford SE, Brockwell DJ, et al. 2020. PyXlinkViewer: a flexible tool for visualization of protein chemical crosslinking data within the PyMOL molecular graphics system. *Protein Science*, **29**(8): 1851–1857.
Spinelli JB, Haigis MC. 2018. The multifaceted contributions of mitochondria to cellular metabolism. *Nature Cell Biology*, **20**(7): 745–754.
Stockwell BR, Angeli JPF, Bayir H, et al. 2017. Ferroptosis: a regulated cell death nexus linking metabolism, redox biology, and disease. *Cell*, **171**(2): 273–285.
Su LJ, Zhang JH, Gomez H, et al. 2019. Reactive oxygen species-induced lipid peroxidation in apoptosis, autophagy, and ferroptosis. *Oxidative Medicine and Cellular Longevity*, **2019**: 5080843.
Sun YX, Zhang J, Yan YJ, et al. 2011. The protective effect of C-phycocyanin on paraquat-induced acute lung injury in rats. *Environmental Toxicology and Pharmacology*, **32**(2): 168–174.
Tan W, Dai FF, Yang DY, et al. 2022. MiR-93–5p promotes granulosa cell apoptosis and ferroptosis by the NF-kB signaling pathway in polycystic ovary syndrome. *Frontiers in Immunology*, **13**: 967151.
Vadiraja BB, Gaikwad NW, Madyastha KM. 1998. Hepatoprotective effect of C-phycocyanin: protection for carbon tetrachloride and *R*-(+)-pulegone-mediated hepatotoxicty in rats. *Biochemical and Biophysical Research Communications*, **249**(2): 428–431.
Wang BQ, Wang Y, Zhang J, et al. 2023. ROS-induced lipid peroxidation modulates cell death outcome: mechanisms behind apoptosis, autophagy, and ferroptosis. *Archives of Toxicology*, **97**(6): 1439–1451.
Wang H, Yu XY, Liu DW, et al. 2024a. VDR activation attenuates renal tubular epithelial cell ferroptosis by regulating Nrf2/HO-1 signaling pathway in diabetic nephropathy. *Advanced Science*, **11**(10): e2305563.
Wang YS, Li BY, Xing YF, et al. 2024b. Puerarin ameliorated PCOS through preventing mitochondrial dysfunction dependent on the maintenance of intracellular calcium homeostasis. *Journal of Agricultural and Food Chemistry*, **72**(6): 2963–2976.
Wu QH, Liu L, Miron A, et al. 2016. The antioxidant, immunomodulatory, and anti-inflammatory activities of Spirulina: an overview. *Archives of Toxicology*, **90**(8): 1817–1840.
Yan HQ, Wang L, Zhang GH, et al. 2024. Oxidative stress and energy metabolism abnormalities in polycystic ovary syndrome: from mechanisms to therapeutic strategies. *Reproductive Biology and Endocrinology*, **22**(1): 159.
Yang FH, Dong XL, Liu GX, et al. 2022. The protective effect of C-phycocyanin in male mouse reproductive system. *Food & Function*, **13**(5): 2631–2646.
Yang WS, Sriramaratnam R, Welsch ME, et al. 2014. Regulation of ferroptotic cancer cell death by GPX4. *Cell*, **156**(1-2): 317–331.
Yilmaz M, Bukan N, Ayvaz G, et al. 2005. The effects of rosiglitazone and metformin on oxidative stress and homocysteine levels in lean patients with polycystic ovary syndrome. *Human Reproduction*, **20**(12): 3333–3340.
Yoshida A, Takagaki Y, Nishimune T. 1996. Enzyme immunoassay for phycocyanin as the main component of spirulina color in foods. *Bioscience, Biotechnology, and Biochemistry*, **60**(1): 57–60.
Yu B, Song C, Feng CL, et al. 2023. Effects of gradient high-field static magnetic fields on diabetic mice. *Zoological Research*, **44**(2): 249–258.
Yu Q, Hao S, Wang H, et al. 2016. Depression-like behavior in a dehydroepiandrosterone-induced mouse model of polycystic ovary syndrome. *Biology of Reproduction*, **95**(4): 79.
Zhang PW, Pan YH, Wu S, et al. 2023. *n*-3 PUFA promotes ferroptosis in PCOS GCs by inhibiting YAP1 through activation of the hippo pathway. *Nutrients*, **15**(8): 1927.
Zhang YL, Swanda RV, Nie LT, et al. 2021. mTORC1 couples cyst(e)ine availability with GPX4 protein synthesis and ferroptosis regulation. *Nature Communications*, **12**(1): 1589.
Zweckstetter M. 2021. NMR hawk-eyed view of AlphaFold2 structures. *Protein Science*, **30**(11): 2333–2337.